รายงานวิจัยฉบับสมบูรณ์

การสังเกตปรากฏการณ์แม่เหล็กเฟอโรที่อุณหภูมิห้องของพอลิเมอร์ที่ปราศจากโลหะ

Room temperature ferromagnetism observation in metal-free polymers

โดย ผศ.ดร. สุปรีดิ์ พินิจสุนทร

กุมภาพันธ์ พ.ศ. 2559

สัญญาเลขที่ MRG5680159

รายงานวิจัยฉบับสมบูรณ์

โครงการ: การสังเกตปรากฏการณ์แม่เหล็กเฟอโรที่อุณหภูมิห้องของพอลิเมอร์ที่ปราศจากโลหะ

Project: Room temperature ferromagnetism observation in metal-free polymers

ผู้วิจัย ผศ.ดร. สุปรีดิ์ พินิจสุนทร
สังกัด ภาควิชาฟิสิกส์ คณะวิทยาศาสตร์ มหาวิทยาลัยขอนแก่น

สนับสนุนโดยสำนักงานกองทุนสนับสนุนการวิจัย

บทคัดย่อ

รหัสโครงการ: MRG5680159

ชื่อโครงการ: การสังเกตปรากฏการณ์แม่เหล็กเฟอโรที่อุณหภูมิห้องของพอลิเมอร์ที่ปราศจากโลหะ

ชื่อนักวิจัย: ผศ.ดร. สุปรีดิ์ พินิจสุนทร มหาวิทยาลัยขอนแก่น

อีเมล : psupree@kku.ac.th

ระยะเวลาโครงการ: 2 ปี

เมื่อไม่นานมานี้มีการทดลองที่แสดงว่าสมบัติแม่เหล็กเฟอโรที่อุณหภูมิห้อง (RT-FM) สามารถถูกเหนี่ยวนำให้เกิดขึ้นได้ในเทฟลอนโดยการดึงหรือตัดอย่างง่าย คำถามที่ตามมาก็คือ ปรากฏการณ์นี้สามารถสังเกตเห็นได้ในพอลิเมอร์ชนิดอื่นๆหรือไม่ ในโครงการวิจัยนี้จึงได้ทำการทดลองหลายๆอย่างเพื่อที่จะแสดงว่าปรากฏการณ์ RF-FM ไม่สามารถเกิดขึ้นได้ในพอลิเมอร์ทุกชนิด ในการทดลอง ได้มีการเปลี่ยนรูปเชิงกลได้แก่การดึงหรือการตัดพอลิเมอร์หลายชนิด (เทฟลอน ยางธรรมชาติ PVDF PP และ พาราฟิล์ม ซึ่งแสดงให้เห็นว่ามีเพียงเทฟลอนและพาราฟิล์มเท่านั้นที่สามารถแสดงสมบัติ RT-FM ในขณะที่พอลิเมอร์ชนิดอื่นๆแสดงสมบัติแม่เหล็กพารา ปรากฏการณ์นี้สามารถอธิบายได้จากการเกิดพันธะคาร์บอนโดดเดี่ยวและการควบคู่แบบแม่เหล็กเฟอโรของพันธะโดดเดี่ยวเหล่านั้น พันธะคาร์บอนโดดเดี่ยวสามารถเกิดขึ้นได้ในพอลิเมอร์ทุกชนิดที่ถูกทำให้เปลี่ยนรูปเชิงกล อย่างไรก็ตามการควบคู่แบบแม่เหล็กเฟอโรระหว่างพันธะคาร์บอนโดดเดี่ยวจะเกิดได้เฉพาะในพอลิเมอร์ที่มีโครงสร้างผลึกและมีระยะห่างระหว่างสายโซ่ประมาณ 5 อังตรอมเท่านั้น ซึ่งก็ได้แก่ เทฟลอนและพาราฟิล์มนั่นเอง โครงการนี้ยังพบว่า ค่าแมกนีไตเซชันของเทฟลอนที่ถูกยืดจะมีค่าสูงขึ้นเมื่อลดอุณหภูมิต่ำลง ซึ่งเป็นสาเหตุมาจากการลดการเคลื่อนไหวของสายโซ่พอลิเมอร์ นอกจากนั้น ความเป็นแม่เหล็กที่ขึ้นกับทิศทางยังสามารถพบได้ในเทฟลอนและพาราฟิล์มที่ถูกตัด ในทั้งสองกรณี แกนง่ายจะพบได้ในทิศทางที่ตั้งฉากกับรอยตัด

คำหลัก: พอลิเมอร์; แม่เหล็กเฟอโร; อุณหภูมิห้อง; พันธะคาร์บอนโดดเดี่ยว;

Abstract

Project Code: MRG5680159

Project Title: Room temperature ferromagnetism observation in metal-free polymers

Investigator: Assist. Prof. Dr. Supree Pinitsoontorn Khon Kaen University

E-mail Address: psupree@kku.ac.th

Project Period: 2 years

It has recently been shown that room temperature ferromagnetism (RT-FM) can be induced in Teflon by simple stretching or cutting. The question was raised whether this is a common phenomenon in any polymer. In this project, several experiments were carried out to show that RT-FM could not be induced in all polymers. Several polymers, i.e. Teflon, natural rubber, PVDF, PP and Parafilm, were mechanically deformed by simply stretching or cutting. Only Teflon and Parafilm exhibited induced RT-FM, whereas other polymers showed paramagnetic behavior. It has been believed that induced RT-FM is caused by a combination of the formation of carbon dangling bonds and ferromagnetic coupling between them. Carbon dangling bonds were generated in all polymers subjected to mechanical deformation. However, ferromagnetic coupling of the carbon dangling bonds could only occur in crystalline polymers with the right chain separation distance (~5 Å), e.g. Teflon and Parafilm. Furthermore, by cooling the stretched Teflon sample, the magnetization was enhanced, which was due to the reduction of dynamic motion of the polymer chains. In addition, magnetic anisotropy could be observed in the cut Teflon and Parafilm. In both cases, the easy axis was found to be in the direction perpendicular to the cut edges.

Keywords : polymers; ferromagnetism; room temperature; carbon dangling bond;

Content

I. Introduction

Ferromagnetism in carbon-based materials is of particular interest for use in lightweight, flexible and cheap magnets. These carbon-based magnets also have potential application in spintronics, since carbon may provide an easy way to integrate spin and molecular electronics [Xia 2008]. However, ferromagnetism in organic materials containing only light elements can be observed only at low temperature (<10 K) [Veciana 2000, Rajca 2001] and so cannot be utilized for any real application. A traditional way to induce room temperature ferromagnetism (RT-FM) in carbon materials is by incorporating metal ions into molecular/organic polymer-based materials [Manriquez 1991, Miller 2000, Jain 2007]. RT-FM in metal-free organic material was discovered in C_{60} subjected to a high-pressure and high-temperature polymerization process [Wood 2002, Han 2003]. Subsequently, RT-FM in other forms of pure carbon has been continuously reported including graphite [Esquinazi 2003, Xia 2008], carbon nanotubes [Friedman 2010] and nanosized diamonds [Talapatra 2005]. In addition, RT-FM was discovered in the aromatic polyimide film Kapton, thermally treated at temperatures between 490 and 540 $^{\circ}$C [Kaburagi 2002]. The observed FM in these carbon-based materials was believed to be of intrinsic origin. An effect from magnetic impurities was ruled out, since no correlation between FM and the magnetic impurity concentration was found [Esquinazi 2002]. The source of FM was attributed to unpaired electrons from defects in the structure. This was also supported by ab initio calculations in a few different carbon systems [Andriotis 2003, Lehtinen 2004, Zanolli 2010].

In observations of RT-FM in carbon-based materials, the samples were treated by a high pressure process [Wood 2002, Han 2003], high temperature post-annealing [Kaburagi 2002, Friedman 2010], or by irradiation [Esquinazi 2003, Talapatra 2005, Xia 2008]. In 2012 Ma et al. reported that RT-FM can be realized in Teflon tape (polytetrafluoroethylene) when subjected to simple stretching and cutting [Ma 2012]. They explained, using first-principle calculation, that the origin of FM was due to carbon dangling bonds and strong ferromagnetic coupling between them. Furthermore, RT-FM was observed in polyethylene by simply cutting the polymer in an inert atmosphere. The experimental results of Ma et al. are of interest since they open up an easy and inexpensive option for creating FM in metal-free polymers. The question now is if these techniques are applicable to other types of polymers. This point is the objective of this study.

Objectives

- Mechanical deform and investigate room temperature ferromagnetism in different polymers, i.e. Teflon tape, natural rubber (polyisoprene), PP (polypropylene), PVDF (polyvinylidene fluoride) and Parafilm (polyethylene).

II. EXPERIMENTAL DETAILS

Five different types of polymers that are easily obtained or commonly used in the lab were selected as the subjects of the experiments. Samples of Teflon tape, Parafilm and PP were purchased whereas natural rubber was prepared by drying commercial latex. PVDF was prepared by polymerization of the monomer in dimethylformamide (DMF) and drying at 60 $^{\circ}$C. Fourier transform infrared spectroscopy (FTIR, Bruker, Tensor27) was used to confirm the functional group of each polymer. To perform the experiment on RT-FM by mechanical deformation, all polymers were cut to have a weight of around 20-40 mg with a length of 30-60 mm and width of 10-18 mm. To avoid any contamination, the samples were carefully handled and a ceramic knife was used for cutting. The polymers were then subjected to mechanical deformation by several means i.e. simple stretching using a Universal Testing Machine (UTM, Instron 5567A) or by hand, or cutting into several pieces, or pinching with a non-magnetic needle. The samples were mounted onto a quartz rod for the magnetic measurements. Details with illustrations of sample preparation and manipulation are shown below (Part I and Part II). The magnetization of the samples at room temperature before and after mechanical deformation was measured using a vibrating sample magnetometer (VSM) option in the Quantum Design VersaLab instrument, USA. Magnetic moment versus temperature measurement was also carried out. To obtain information on the crystallinity of each polymer, samples were characterized using X-ray diffraction (XRD) with an X-ray diffractometer employing Cu Kα radiation (Bruker, D2 PHASER). Furthermore, all polymers were subjected to elemental analysis using energy-dispersive X-ray spectroscopy (EDS) equipped on the scanning electron microscope (SEM, SEC SNE-4500M). In addition, electron spin resonance (ESR) spectra for inspection of unpaired electrons were obtained using an ESR spectrometer (JEOL, JES-RE2X).

Part I. Schematic illustrations, with the corresponding experimental set up images, of several mechanical deformations in Teflon tape: (a) Unstretched (b) Tensile stretched (c) manually stretched (d) cut (e) pinched

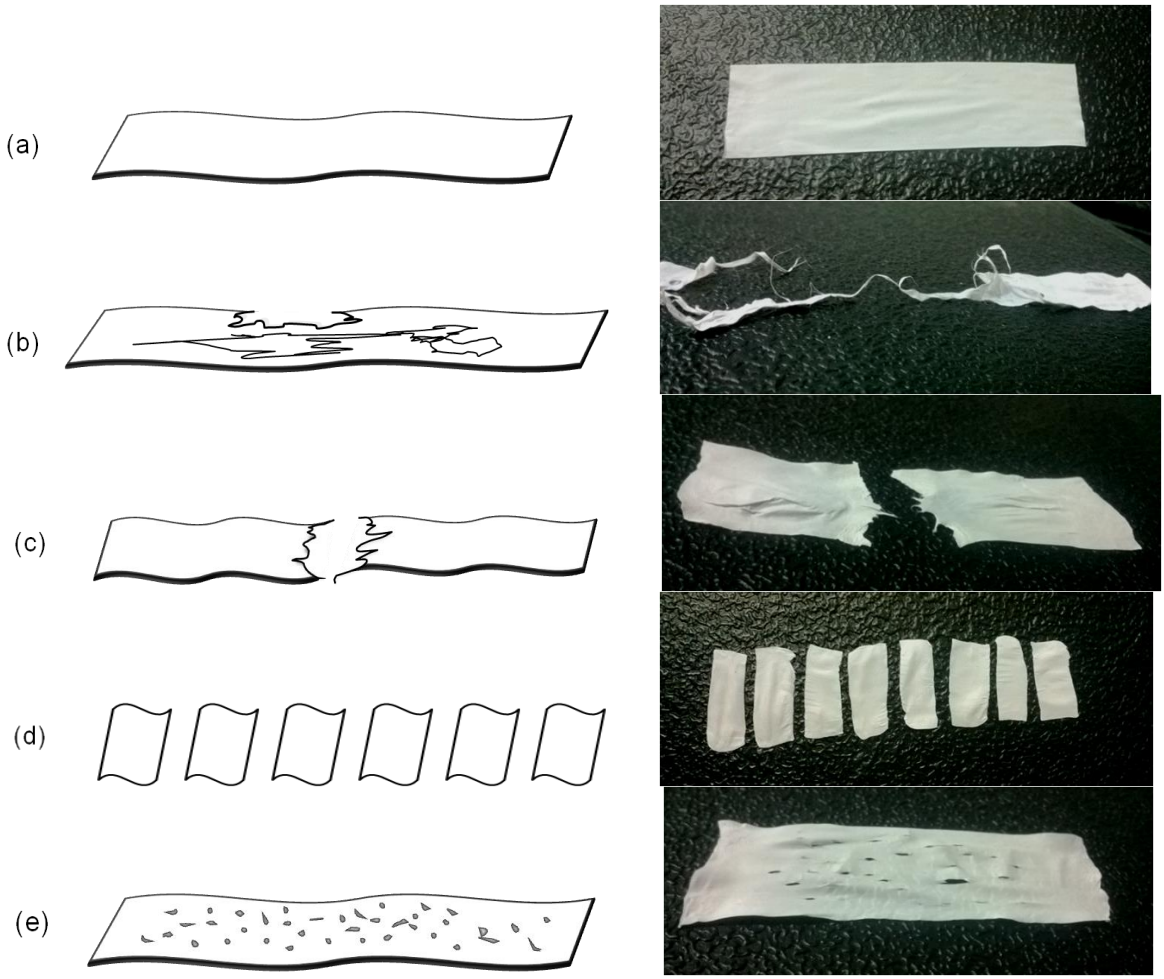

Part II. Illustration of sample preparation and manipulation for the magnetic measurment.

Part II A. Typical procedure for handling the stretched sample for magnetic measurement

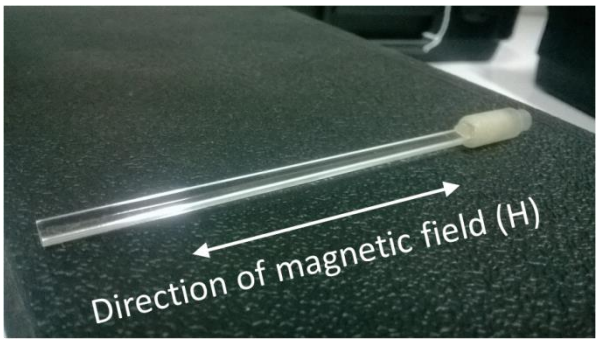

VSM rod made of quartz (very low magnetic background)

Stretched Teflon tape and the VSM rod

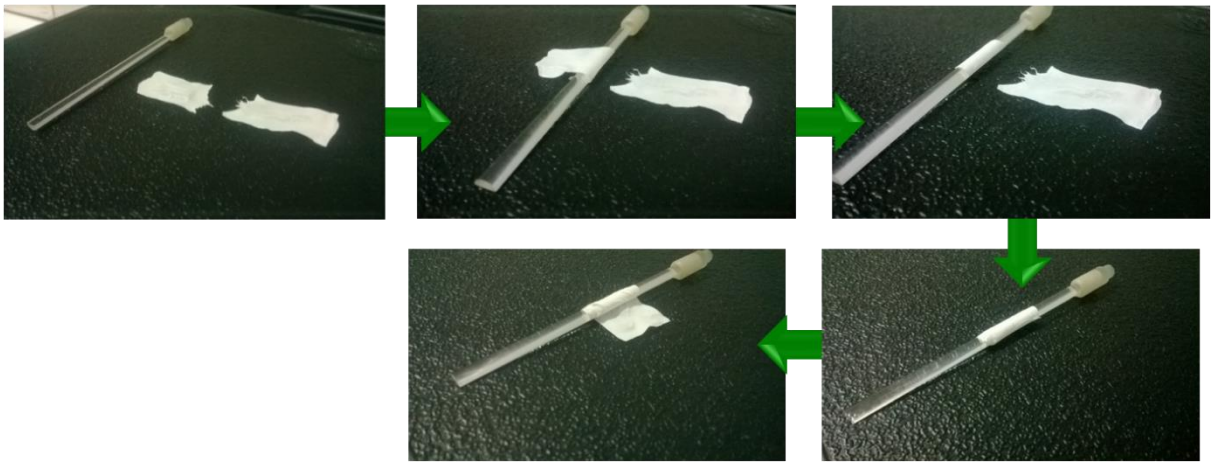

Typical method for mounting samples onto the rod

Part II B. Typical procedure for handing the cut samples for magnetic measurement

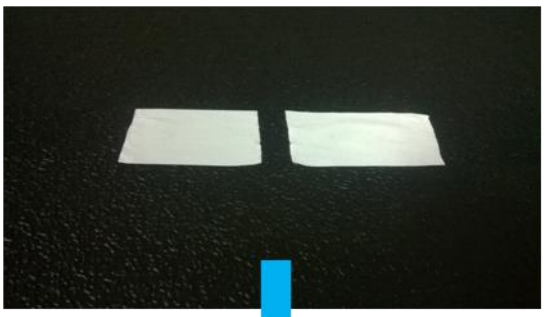

Cut samples into 2 pieces

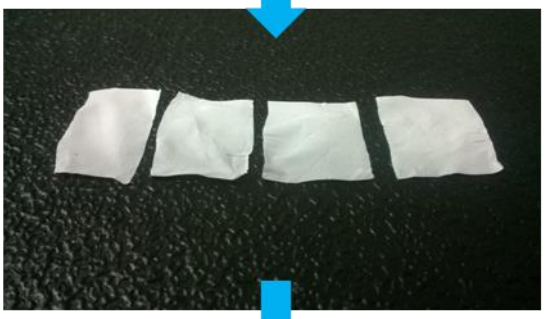

Cut samples into 4 pieces

Cut samples into 8 pieces

The cut samples ready to be mounted onto the VSM rod

For magnetic anisotropy measurement, two types of sample mounting procedure were carried out:

1. Mounting samples of which the cut edges are aligned perpendicularly to the magnetic field direction

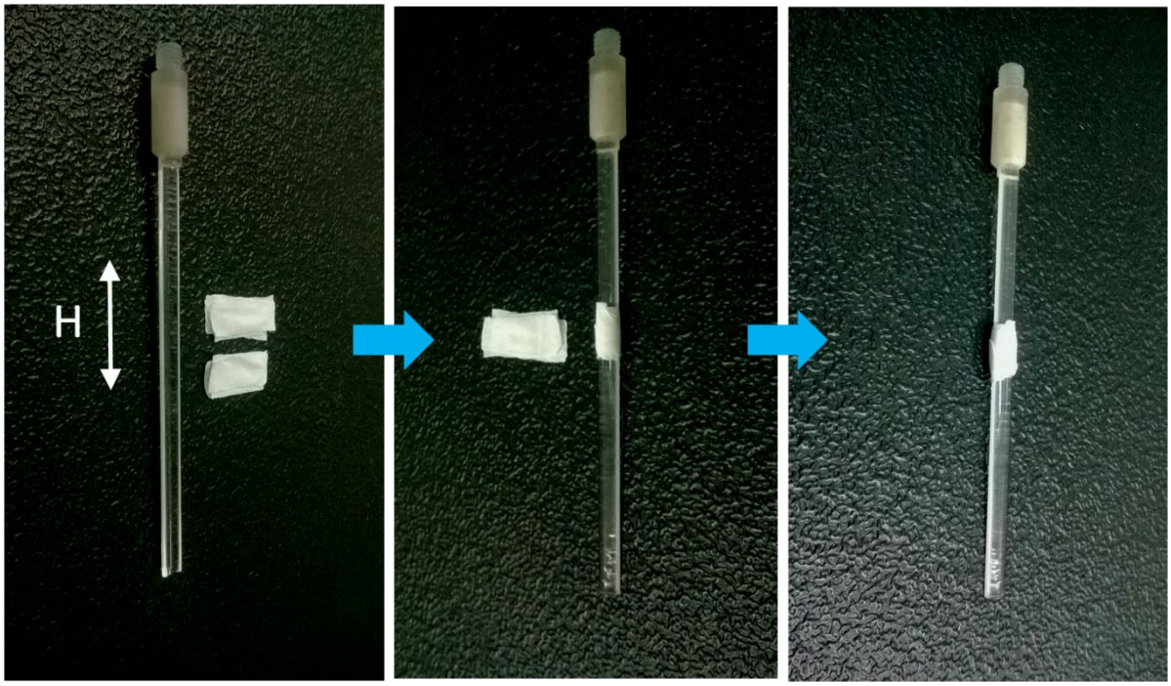

2. Mounting samples of which the cut edges are aligned perpendicularly to the magnetic field direction

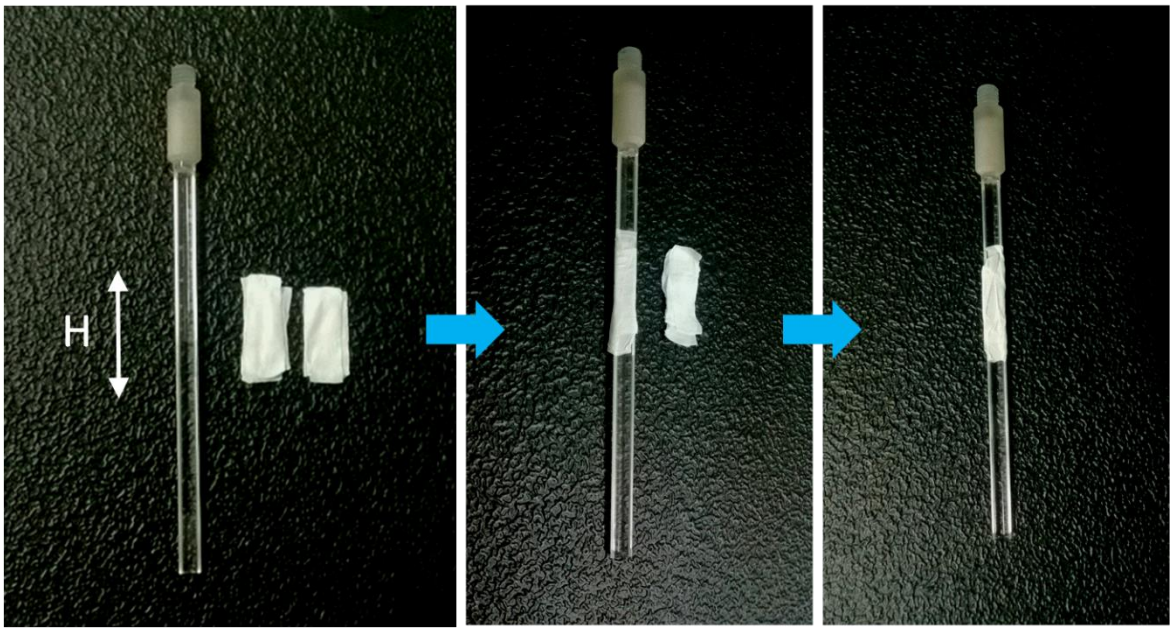

III. RESULTS AND DISCUSSION

We started our experiment by investigating RT-FM in Teflon tape, similarly to the experiments of Ma et al. [Ma 2012]. The result of the M-H curve measurement of the as-prepared unstretched Teflon tape is shown in Fig. 1. A typical diamagnetic characteristic was observed. The RT-FM of Teflon tape was induced by simply stretching by hand as shown in the red circle curve in Fig. 1. The result at this point resembled to the work done by Ma et al. [Ma 2012]. According to Ma et al. [Ma 2012], the observed RT-FM can be attributed to carbon dangling bonds and their ferromagnetic coupling.

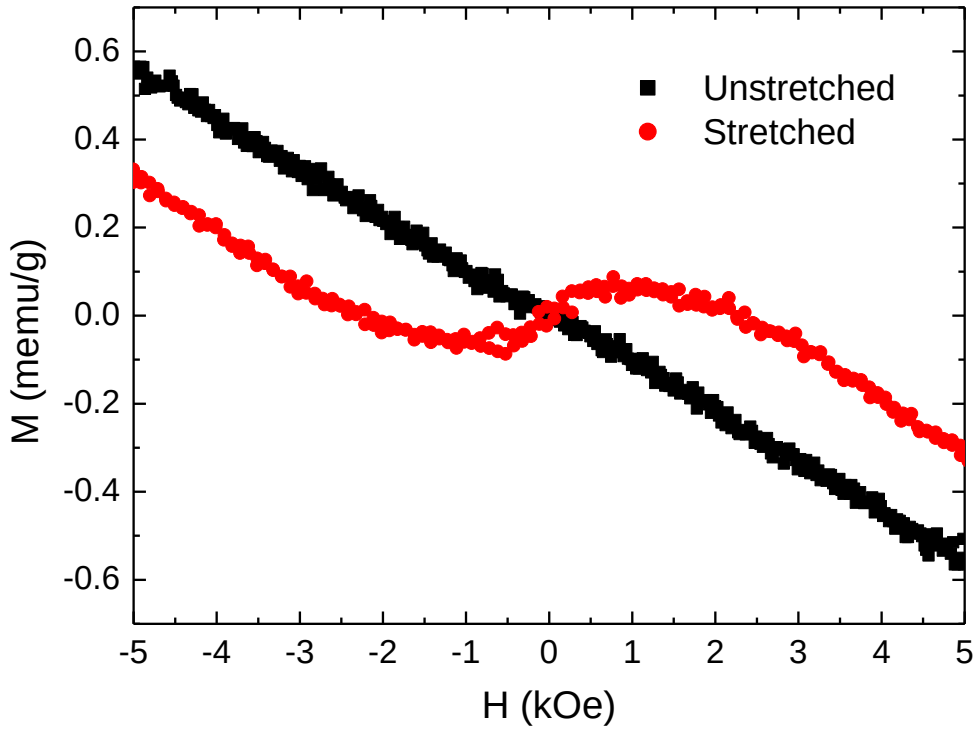

Fig. 1. Room temperature M-H curves of unstretched and stretched Teflon tape (without diamagnetic subtraction)

We further investigated whether other types of mechanical deformation could affect the RT-FM of the Teflon tape. The results are shown in Fig. 2a, which demonstrates the M-H loops of the Teflon tape subjected to many kinds of deformations. RT-FM of the mechanically deformed Teflon tape can be found in all treatments. The strongest ferromagnetic signal was found in Teflon tape subjected to tensile stretching using the Universal Testing Machine (UTM). This is because the UTM can uniformly stretch the sample and possibly generate a larger

number of dangling bonds compared to the other methods. In fact, the magnetization value in our case is much greater than that reported by Ma et al. [Ma 2012]. This may be due to the severe deformation of the Teflon tape by tensile stretching in our case (see the image in the supplementary information), which probably creates more dangling bonds. The samples cut into small pieces also show the RT-FM signal (Fig. 2b). The inset of Fig. 2b shows the variation of saturation magnetization (M_s) as a function of the number of cuts. Pinching the samples with a non-magnetic needle can induce RT-FM, but the signal is much smaller than for the stretched or cut samples. The easiest method in producing RT-FM in Teflon is by simply stretching the sample by hand (manually stretched in Fig. 2b). Since this is the simplest method, the RT-FM in polymers in the following texts is induced by manually stretching, unless stated otherwise. In all cases, the coercivity is very low (< 100 Oe). Note that the M-H curves in Fig. 2 were processed by removing the diamagnetic signals. The slope of the diamagnetic part was calculated and used for background subtraction. After removing the diamagnetic signals, only the FM signals were observed for the mechanically deformed samples and a flat curve near zero was observed for the unstretched sample.

The stability of the RT-FM of the stretched Teflon tape was tested by measuring the magnetic properties after exposing the tensile stretched samples to normal atmosphere for several days. The results are presented in Fig. 2c. It can be seen that the magnetization gradually decreased from the first day to day 9. As was mentioned that the origin of FM in Teflon is due to the carbon dangling bonds, these dangling bonds may not be stable in normal atmosphere. It is possible that oxygen or water molecules (due to the high humidity in Thailand) may be absorbed and saturate the dangling bonds, eliminating FM [Ma 2012]. Next, the stability of RT-FM under the influence of different solutions was tested. The stretched Teflon was submerged in water, ethanol or acetone and measured the M-H curves as shown in Fig. 2d. It can be seen that the solution did not affect the magnetization, which may be due to the low permeability of these solutions in Teflon. Therefore, the dangling bonds were untouched and the RT-FM was unchanged.

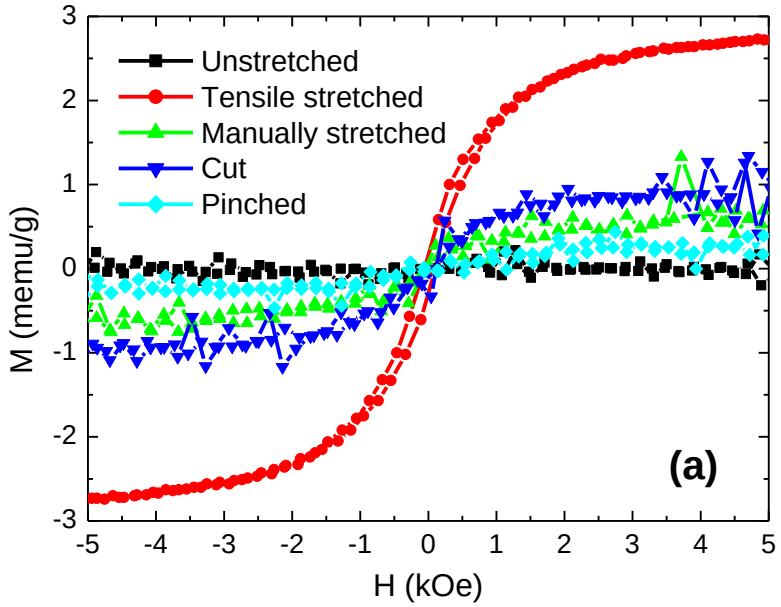
Unstretched
Tensile stretched
Manually stretched
Cut
Pinched
(a)
M (memu/g)
H (kOe)

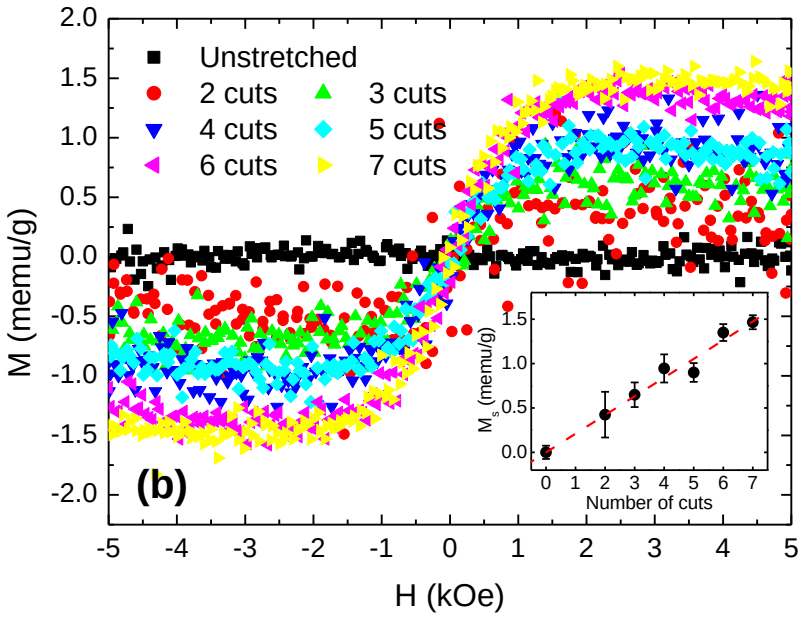
Unstretched
2 cuts
3 cuts
4 cuts
5 cuts
6 cuts
7 cuts
(b)
M (memu/g)
H (kOe)
M_s (memu/g)
Number of cuts

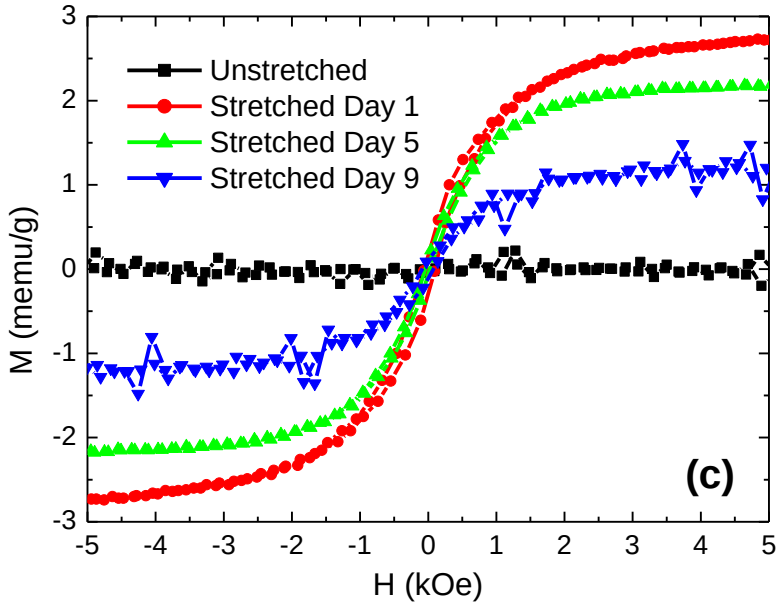
Unstretched
Stretched Day 1
Stretched Day 5
Stretched Day 9
(c)
M (memu/g)
H (kOe)

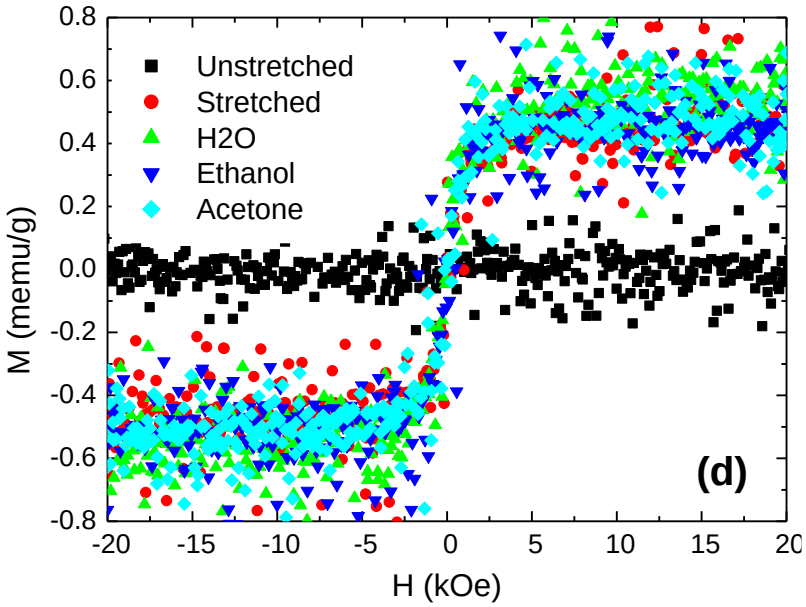

Fig. 2. Room temperature M-H curves of (a) Teflon subjected to several mechanical deformations, (b) Teflon tape as a function of number of cuts (inset shows saturation magnetization (M_s) versus the number of cuts), (c) tensile stretched Teflon after being left in a normal atmosphere, and (d) stretched Teflon after being submerged in different solutions. In every curve, the diamagnetic signals were subtracted from the raw data.

Furthermore, the temperature dependence of magnetization in the stretched Teflon was tested. The results are presented in Fig. 3. The magnetization at low field (500 Oe) is relatively independent of temperature until the temperature was cooled down below 100 K. The magnetization rose up steeply from 80 to 50 K. This is in an agreement with the M-H curves (without diamagnetic subtraction) of the stretched Teflon at several temperatures as shown in the inset of Fig. 3. The change in magnetization with temperature can be related to the dynamic motion of the polymer chain. At RT, there can be large movement of polymer chain due to thermal fluctuation. This would reduce the ferromagnetic coupling. On the other hand, the chain dynamic motion is limited at lower temperature. The ferromagnetic coupling would be enhanced, resulting in higher magnetization. On the other hand, the M-T measurement for the unstretched Teflon does not show any dependence of T on M. It should be noted that it would be very interesting to study the dependence of magnetization for the stretched sample at even lower temperature. Unfortunately this could not be carried out in the present study because of the limitations of our instrument.

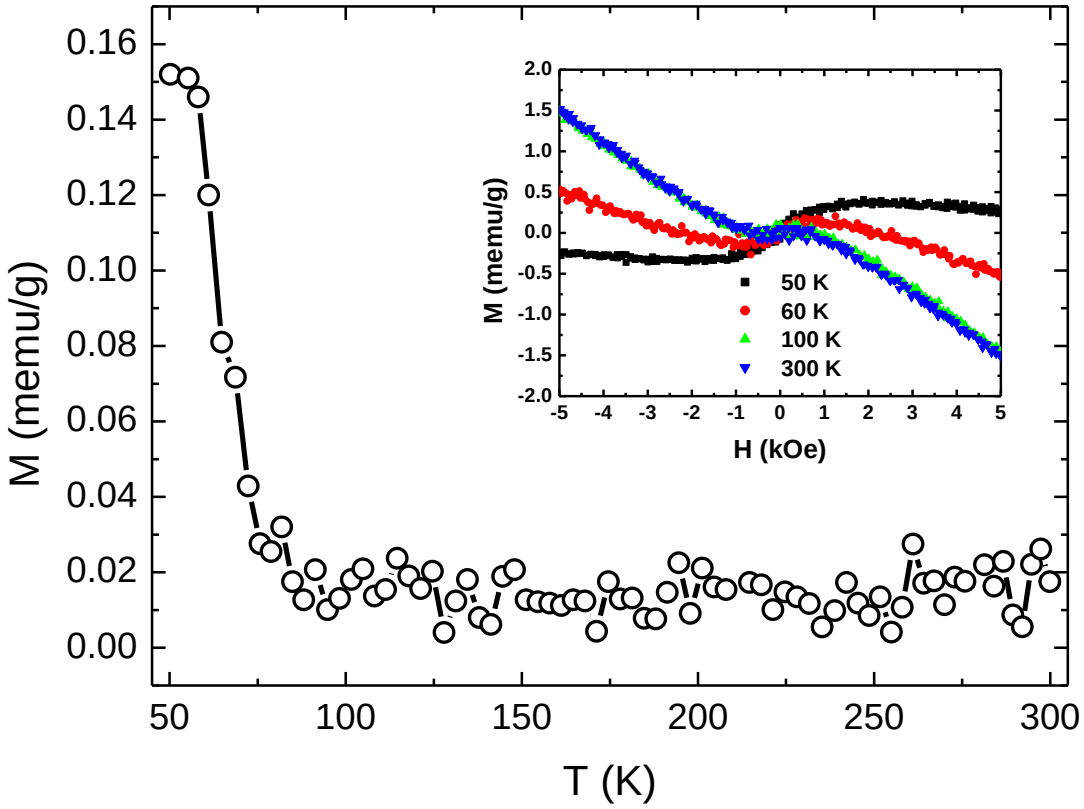

Fig. 3. Temperature dependence of magnetization for stretched Teflon at a magnetic field of 500 Oe. Inset: M-H curves at several temperatures.

After the FM observation in Teflon, the investigation was moved to other polymers. The FTIR spectrum of each sample was obtained to confirm the functional groups of the polymers used in this study. The FTIR results are shown in Fig. 4.

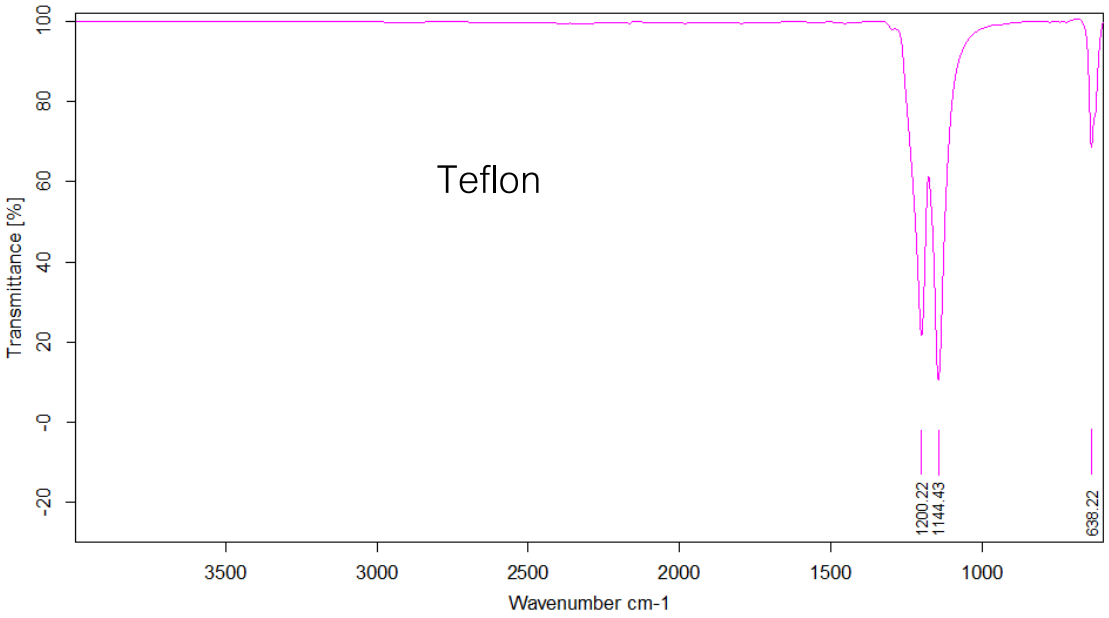

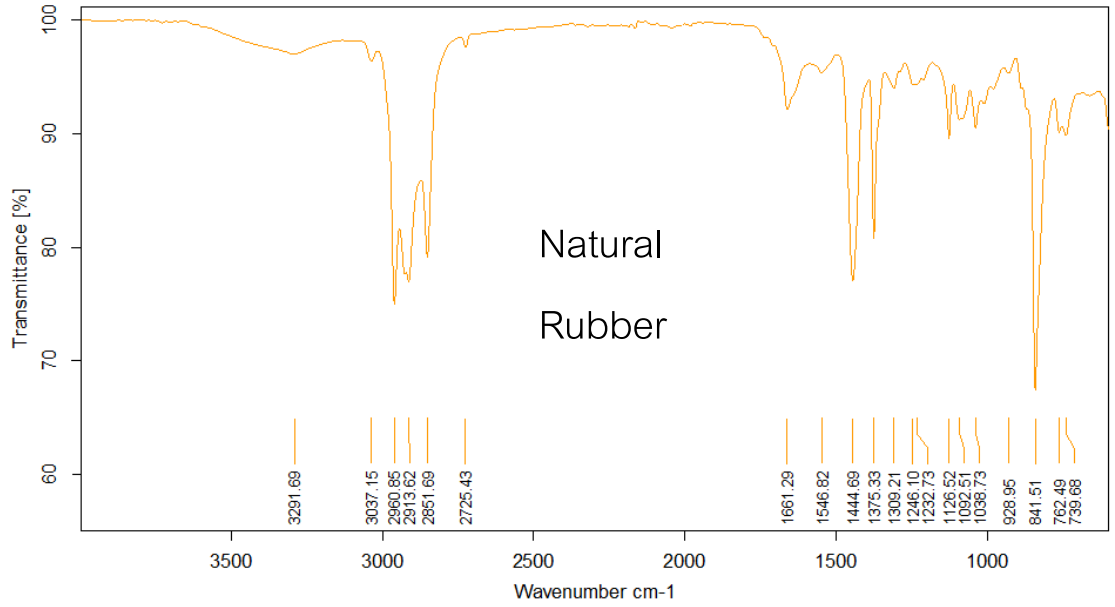
Natural
Rubber
Transmittance [%]
Wavenumber cm-1
3291.69
3037.15
2960.85
2913.62
2851.69
2725.43
1661.29
1546.82
1444.69
1375.33
1309.21
1246.10
1232.73
1126.52
1092.51
1038.73
928.95
841.51
762.49
739.68

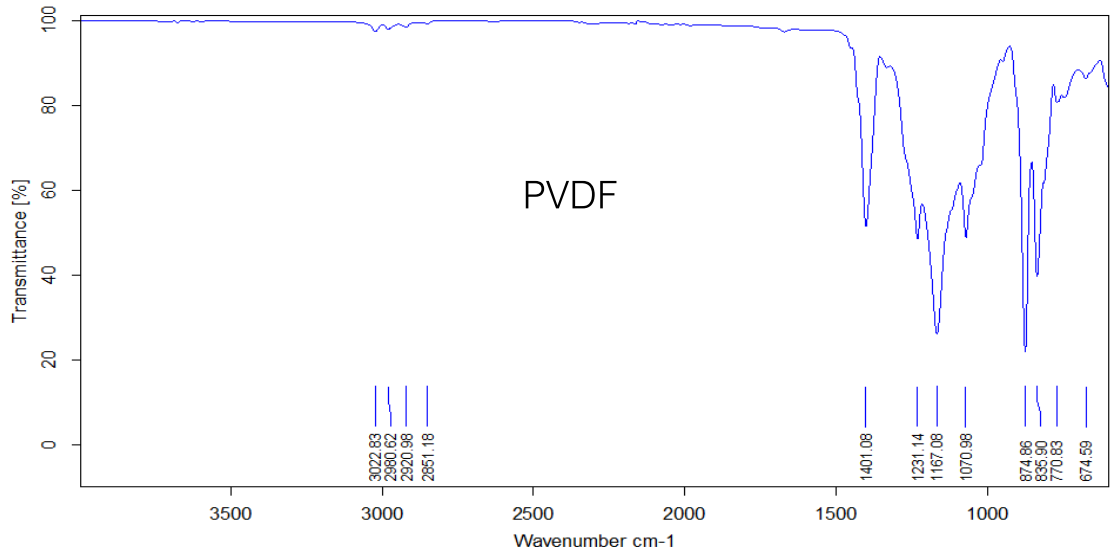
PVDF
Transmittance [%]
Wavenumber cm-1
3022.83
2980.62
2920.98
2851.18
1401.08
1231.14
1167.08
1070.98
874.86
835.90
770.83
674.59

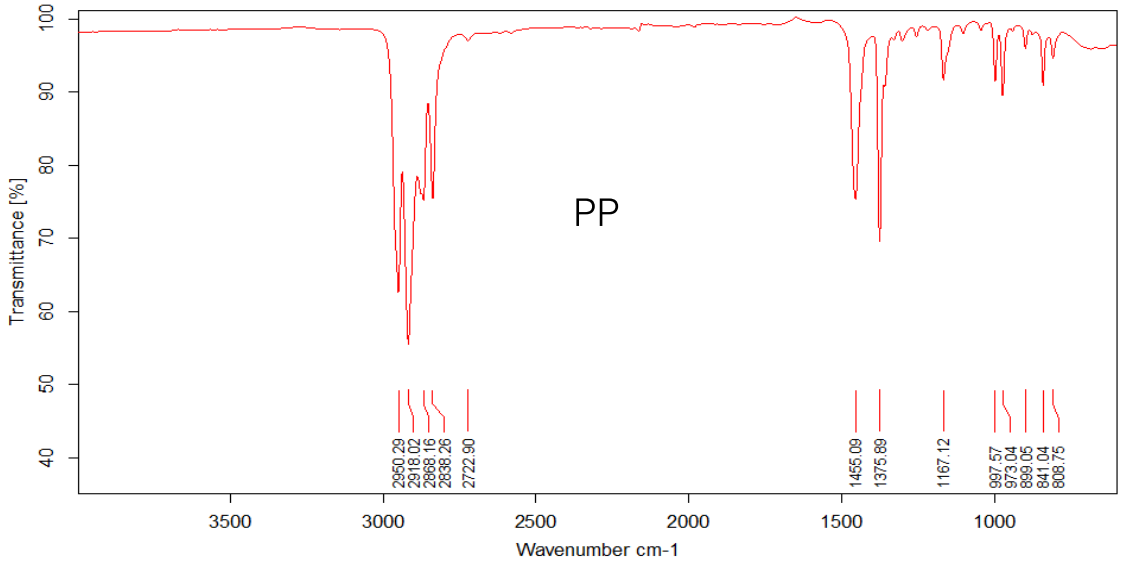
PP
Transmittance [%]
Wavenumber cm-1
2950.29
2918.02
2868.16
2838.26
2722.90
1455.09
1375.89
1167.12
997.57
973.04
899.05
841.04
808.75

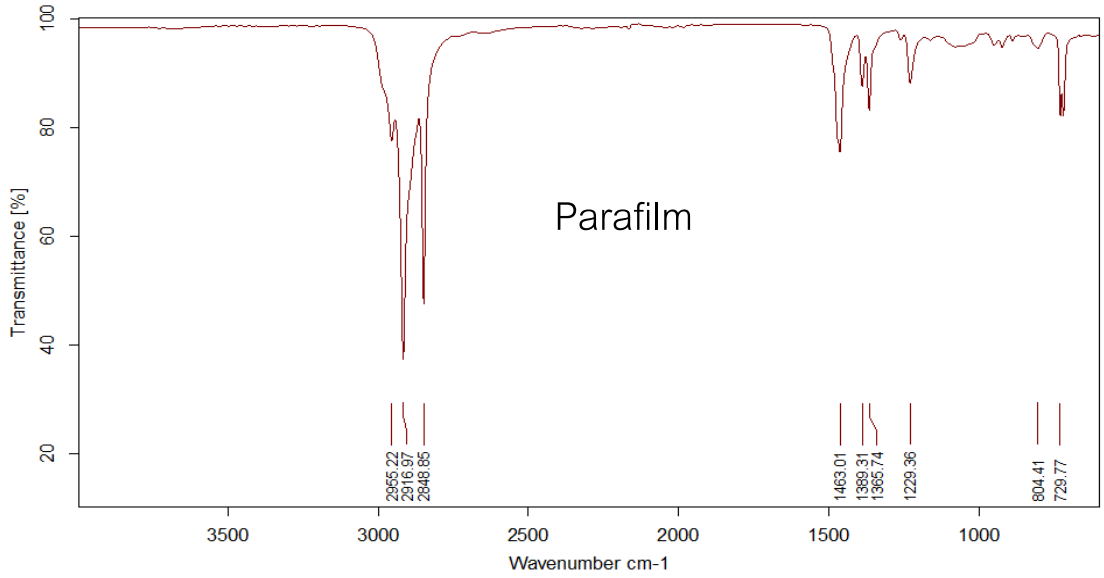

Fig. 4. FTIR spectra (Bruker, Tensor27) of the unstretched polymers used in the experiments.

Fig. 5 shows the M-H curves of the investigated polymers after diamagnetic signal subtraction. For natural rubber, PP and PVDF, RT-FM was not observed. PVDF was chosen because the chain structure of PVDF $(-CF_2-CH_2-)_n$ is similar to Teflon $(-CF_2-CF_2-)_n$. The absence of RT-FM in PVDF indicates that the ferromagnetic behavior is irrelevant to the C-F bonds or their related interaction. However, Fig. 5 shows the change in the slopes of the graph for the stretched natural rubber, PP and PVDF, compared to the unstretched samples. The positive slopes of the M-H curves indicate paramagnetism. From these results, it can be interpreted that stretching the natural rubber, PP and PVDF results in the formation of carbon dangling bonds as a source of available magnetic moments ($1\mu_B$ per 1 dangling bond). However, the lack of ferromagnetic coupling of these dangling bonds suppresses the RT-FM in such polymers. On the other hand, Fig. 5d shows the M-H curves of the unstretched, stretched and cut Parafilm. It is obvious that stretching or cutting Parafilm results in the characteristic S-shape curves of ferromagnetic materials. The inset of Fig. 5d shows the variation of saturation magnetization (M_s) as a function of the number of cuts. The origin of the RT-FM in Parafilm is also attributable to the ferromagnetic coupling of carbon dangling bonds. This part of our experiment shows that RT-FM is not observed in all polymers by simply stretching or cutting. Only some polymers exhibit this behavior, i.e. Teflon and Parafilm. Hence, there must be other influential factors for inducing RT-FM.

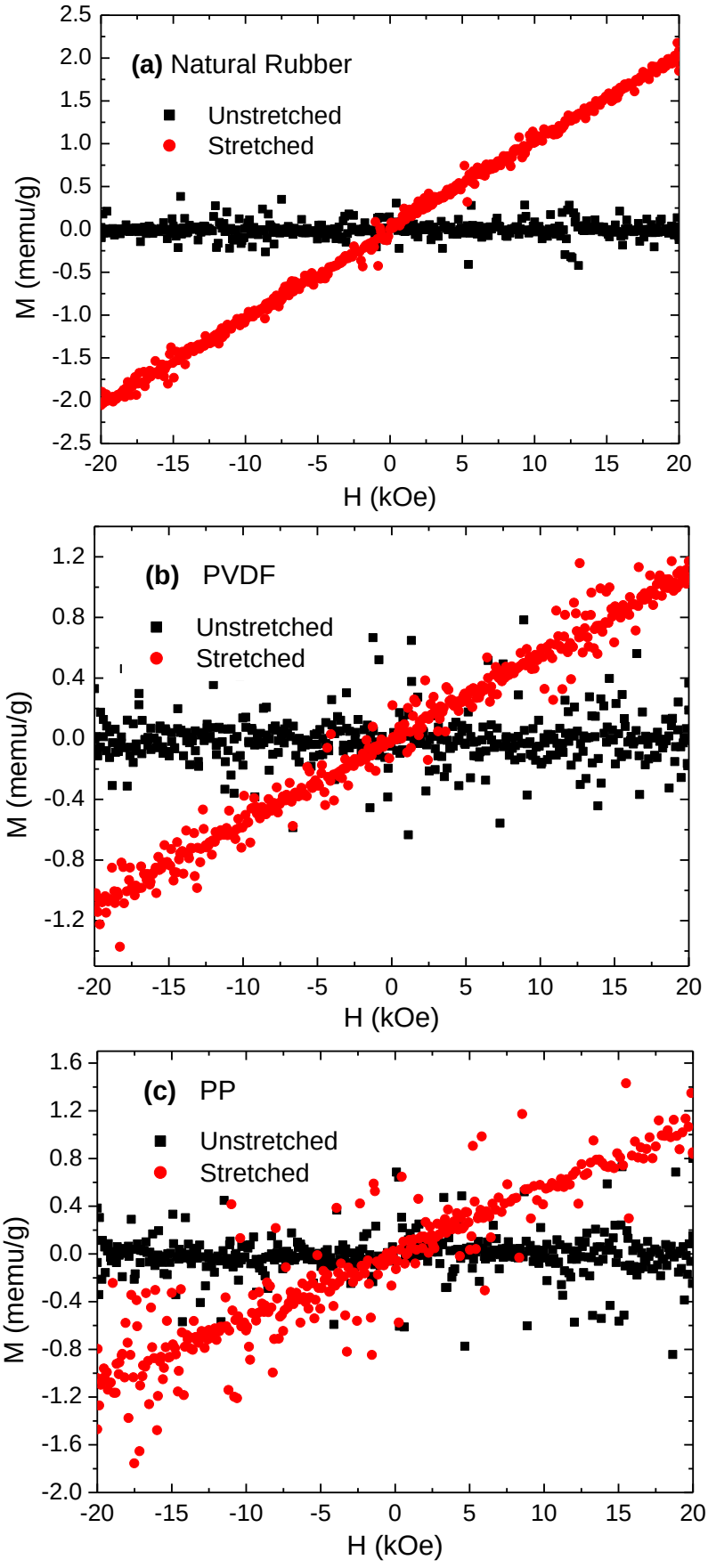
(a) Natural Rubber
Unstretched
Stretched
M (memu/g)
H (kOe)
(b) PVDF
Unstretched
Stretched
M (memu/g)
H (kOe)
(c) PP
Unstretched
Stretched
M (memu/g)
H (kOe)

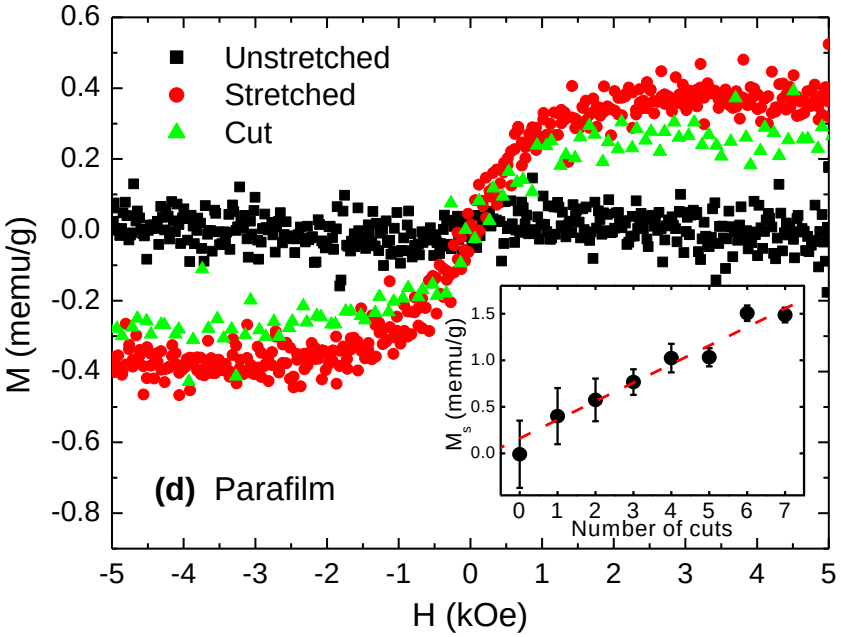

Fig. 5. Room temperature M-H curves of several polymers subjected to simple stretching or cutting: (a) Natural rubber, (b) PP, (c) PVDF and (d) Parafilm, inset shows saturation magnetization (M_s) versus the number of cuts. In every curve, the diamagnetic signals were subtracted from the raw data.

To answer the question, the XRD patterns of the unstretched polymers used in the experiment were measured as shown in Fig. 6. The XRD patterns of the unstretched and stretched polymers were found to be insignificantly different. The XRD pattern of the Teflon sample can be matched with JCPDS card (47-2217), corresponding to the pseudo-hexagonal structure with a=b=5.66 Å, similarly to a previous report [Bunn 1954]. The very sharp peak at 2θ = 18.10° indicates the high crystallinity of the sample. For natural rubber and PVDF, broad XRD spectra were observed, implying mostly an amorphous structure. One of the reasons that RT-FM was not found in natural rubber or PVDF may be due to the absence of crystallinity. For PP and Parafilm, crystalline peaks can be observed on the amorphous background in both samples. If the crystalline structure of polymers is the reason for ferromagnetic coupling, both samples should exhibit ferromagnetic behavior. However, RT-FM was only observed in Parafilm but not PP. The crystalline part of the PP sample can be matched with the JCPDS card (50-2397) corresponding to the monoclinic structure with the lattice parameters of a=6.63 Å, b=20.78 Å and c=6.50 Å. The XRD pattern of Parafilm can be related to the orthorhombic polyethylene structure with a=7.40 Å, b=4.93 Å and c=2.54 Å, JCPDS card (53-1859). Ma et al.

used the first principle calculation to show that the ferromagnetic coupling is energetically favourable only when the chain separation is around 5 Å [Ma 2012]. Our XRD results show that only Teflon and Parafilm fall in this criterion, which leads to ferromagnetic coupling of carbon dangling bonds after stretching or cutting.

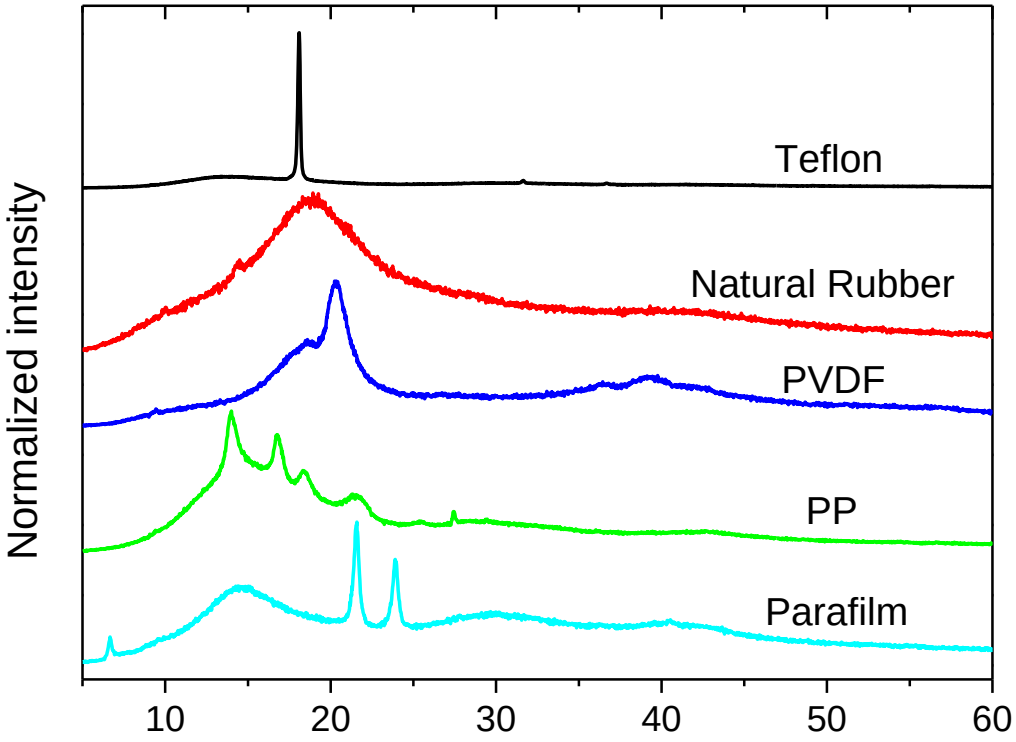

Fig. 6. XRD patterns of the unstretched polymers used in this research.

To ensure that the ferromagnetic signals of Teflon and Parafilm are from the intrinsic origin, energy dispersive X-ray spectra of the unstretched and stretched samples were measured. The metallic impurity was not found in all the spectra (Fig. 7 and 8). The detection limit of the EDS is typically about 1000 ppm by weight. Therefore, using the EDS alone may not be able to distinguish FM from impurity sources. However, it is still confident that the origin of RT-FM in the particular polymers is intrinsic. Several reasons support this argument. Firstly, the difference in magnetic behavior before and after stretching Teflon (and Parafilm), using the same piece of sample, can be clearly observed. Secondly, the saturation magnetization values of Teflon (Fig. 2b) and Parafilm (Fig. 5d) increase as a function of number of cuts, indicating that the larger number of dangling bonds can directly affect the FM behavior. Finally, the magnetization of the stretched Teflon decreases with time (Fig. 2c). The combination of all this evidence can effectively reject the existence of metallic impurities and verify the intrinsic origin of the RT-FM.

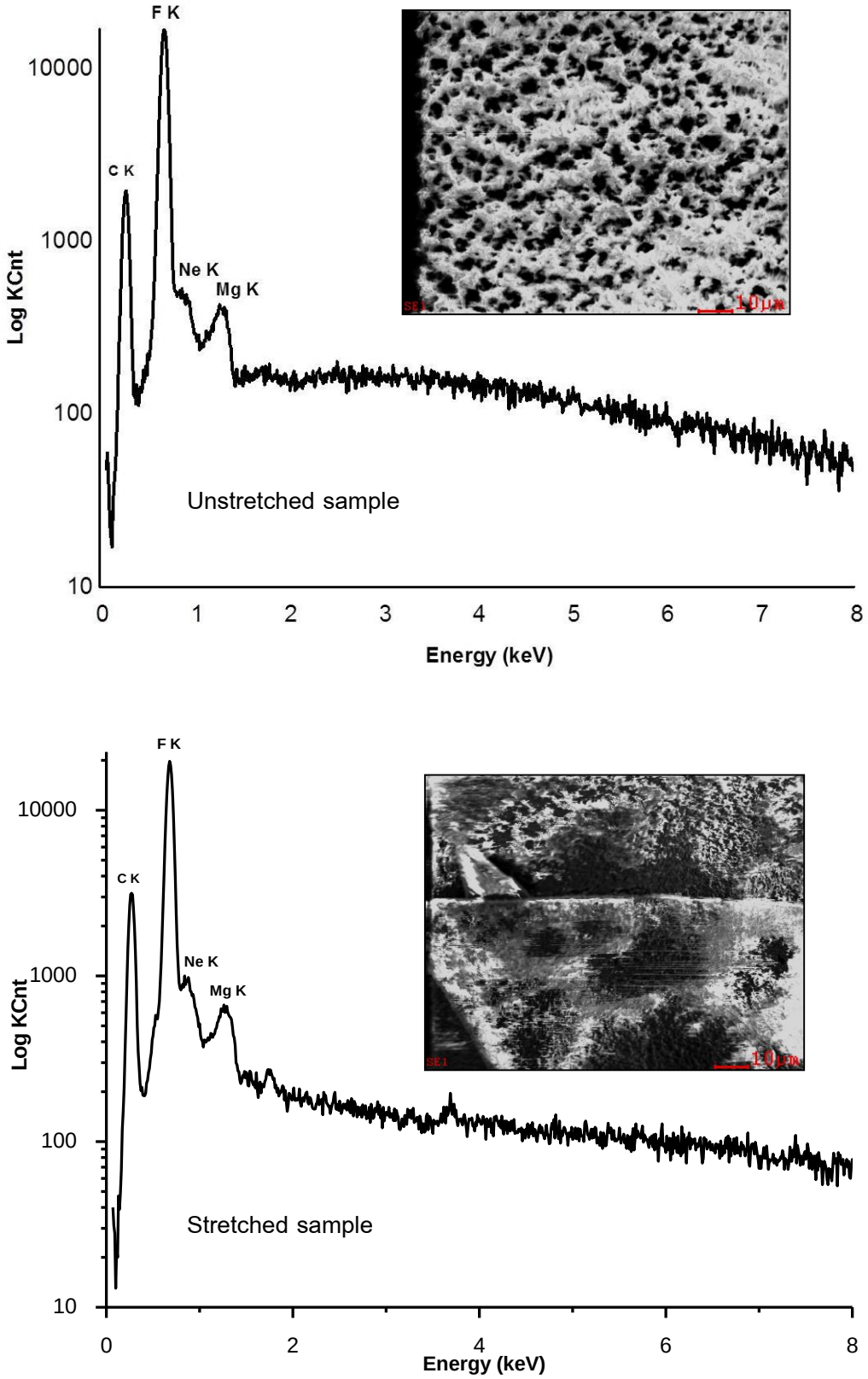

Fig. 7 Typical EDX spectra (SEC, SNE-4500M), with the corresponding SEM images, of the Teflon used in the experiment. The detected elements are mainly C and F. The other detected elements are Ne and Mg which are not magnetic materials.

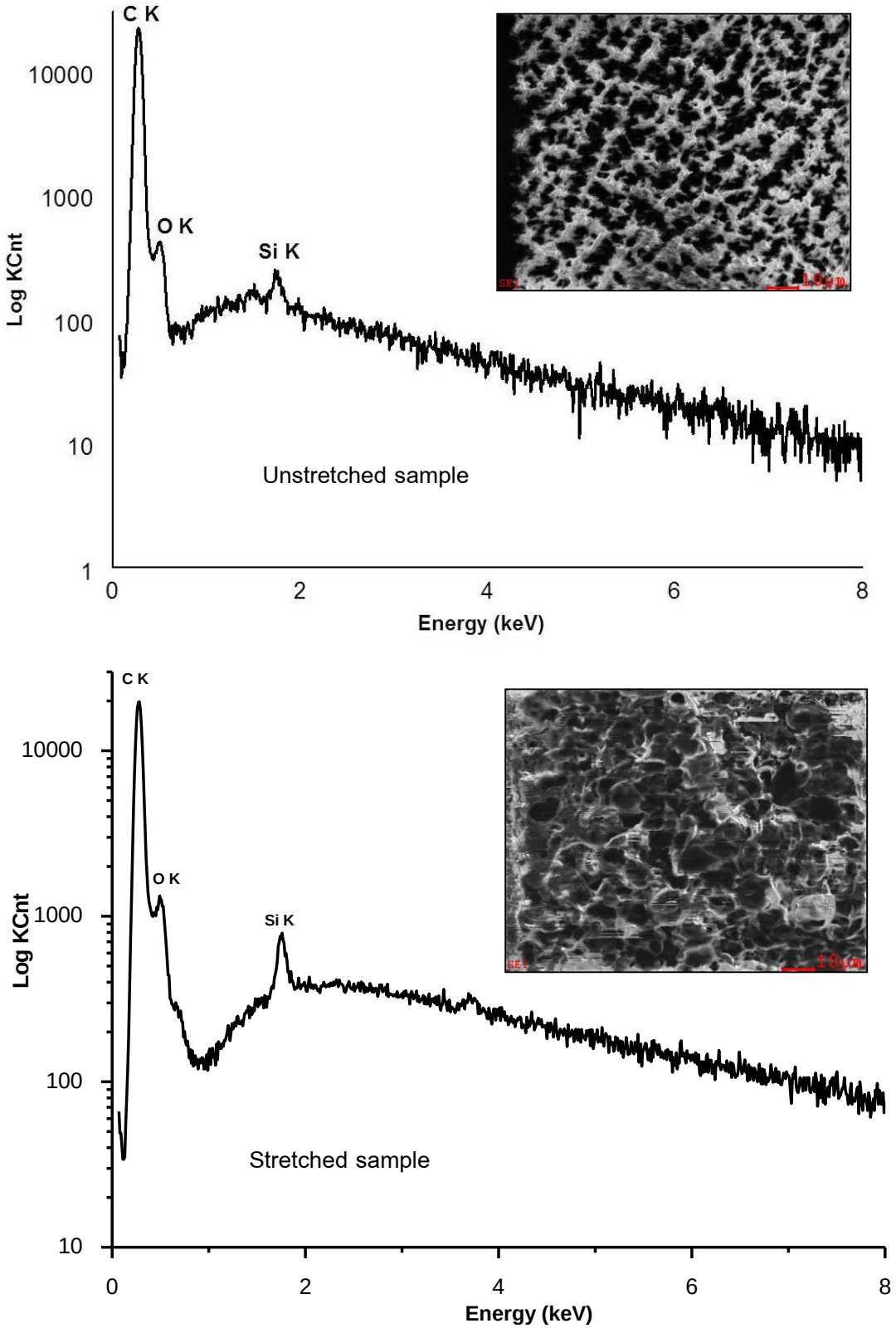

Fig. 8. A typical EDX spectrum (SEC, SNE-4500M), with the corresponding SEM image, of the Parafilm used in the experiment. The detected elements are mainly C. The other detected elements are O and Si which are not magnetic materials.

In this work, it has been shown that by simple stretching or cutting or other form of mechanical deformation, the RT-FM of Teflon and Parafilm can be created. However, this RT-FM cannot be generated for any polymer in general. A guideline for observing RT-FM in polymers is suggested as follows. (1) The polymer must be mostly crystalline. Stretching or cutting amorphous polymers can result in formation of isolated dangling bonds without any magnetic interaction. This would thus induce only paramagnetism. (2) The separation between the chains of the polymer must be at the right distance (around 5 Å). A smaller distance results in antiferromagnetic coupling, whereas for further separation, no magnetic exchange coupling exists.

The ESR spectra (first derivative) of each polymer are shown in Fig. 9. ESR spectroscopy is a technique for studying materials with unpaired electrons. At the right combination of frequency and magnetic field values, the unpaired electrons can switch between their two spin states (the lower and upper states). Hence, ESR spectra can be used to detect the existence of unpaired electrons in the materials. The intensity of the signal depends on the concentration of the unpaired electrons. From Fig. 9, it is clearly seen that the strongest change in the ESR spectra occurs between unstretched and stretched Natural Rubber. However, Natural Rubber does not exhibit RT-FM due to its lack of crystallinity. The smallest signals are observed from PVDF and PP, and the signals are nearly unchanged between the stretching states. This is the reason the RT-FM was not observed in these polymers. As discussed earlier, RT-FM can be induced in stretched Teflon and Parafilm due to the formation of carbon dangling bonds; ESR results show strong evidence to support this. Teflon and Parafilm show changes in ESR signals between stretching states, indicating the creation of dangling bonds in the stretched state. In combination with their crystallinity, RT-FM can be induced in these polymers. It should be noted that ESR signals can always be found in unstretched polymer. This is because very small pieces of polymers are needed in the test tube for the ESR measurement. Cutting polymer into small pieces always creates some dangling bonds, which could be the source of the ESR signals.

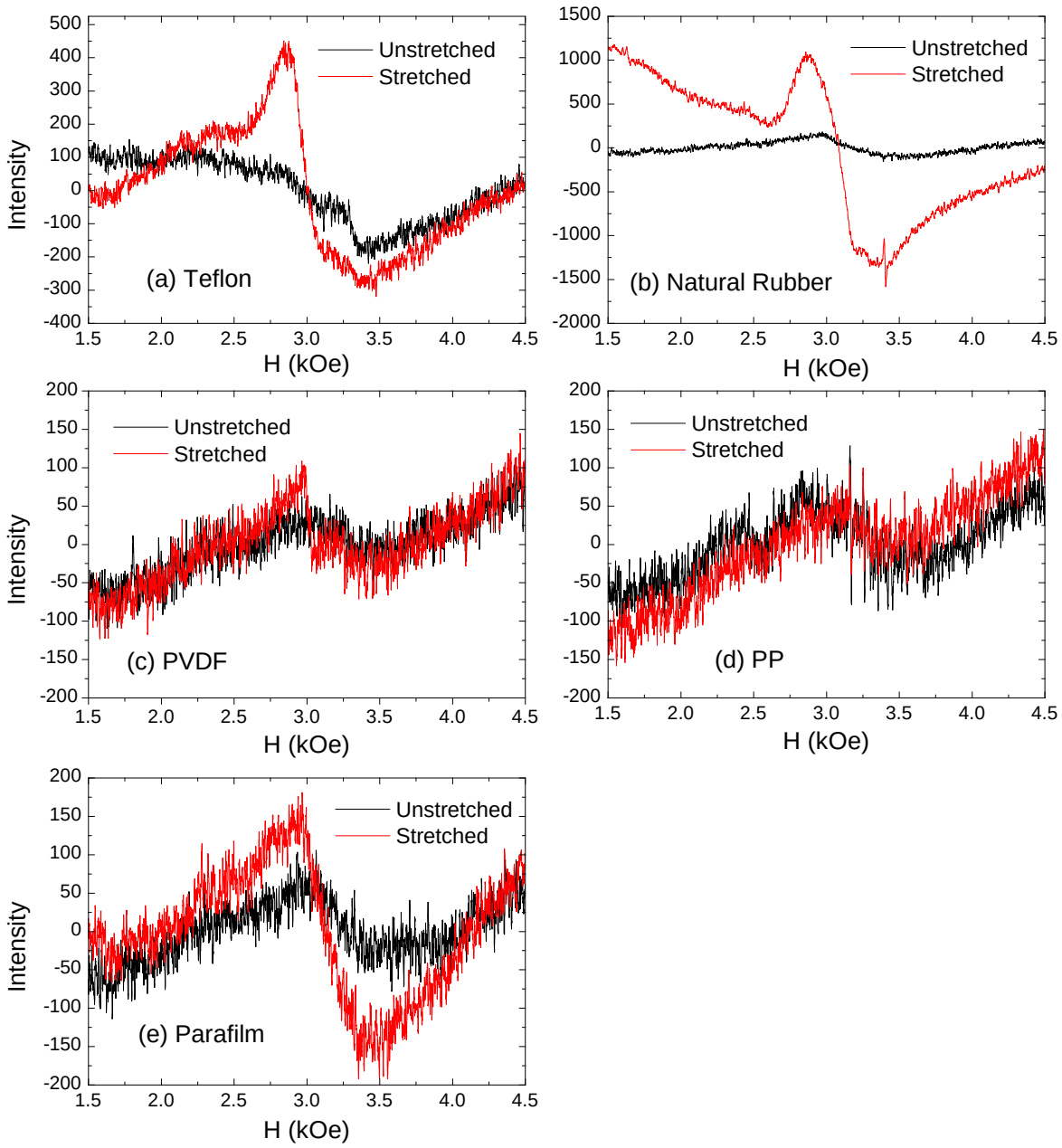

Fig. 9. Comparison of ESR spectra between unstretched and stretched polymers: (a) Teflon, (b) Natural Rubber, (c) PVDF, (d) PP, (e) Parafilm.

In addition, from the above discussion, the created dangling bonds and their magnetic interactions could be dependent on the magnetic field direction; in other words, magnetic anisotropy could be observed. To test this assumption, the Teflon tapes (and Parafilm) were cut into several small pieces. In one set, the samples were aligned such that their cut edges were perpendicular to the magnetic field. In the other set, the cut edges of the samples were parallel to the field. The results are shown in Fig. 10. It is obvious that an anisotropic effect can be

observed. In both Teflon and Parafilm cases, the samples that had their cut edges aligned perpendicularly to the field exhibited higher magnetization, indicating that the easy axis is in the direction perpendicular to the cut edges.

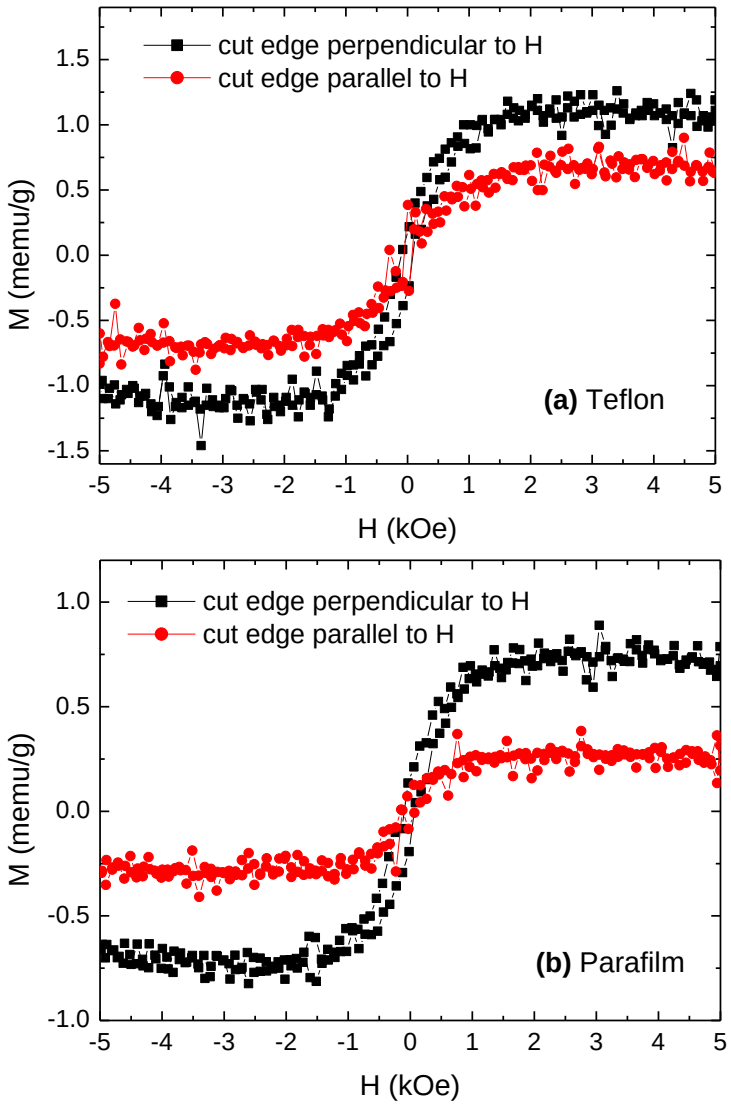

Fig. 10. Magnetic anisotropic behavior of Teflon and Parafilm when the applied field is perpendicular or parallel to the cut edge.

IV. CONCLUSION

In this work, it has been shown that RT-FM is not a common phenomenon in all polymers. By mechanically stretching or cutting several polymers, RT-FM could be induced only in Teflon tape and Parafilm. Natural rubber, PVDF and PP, on the other hand, exhibited paramagnetic behavior. It was proposed that RT-FM can only be observed in some polymers that are highly crystalline, with a chain separation distance of around 5 Å (Teflon and Parafilm). When these polymers were stretched or cut, carbon dangling bonds were generated. With the right chain separation distance, the dangling bonds couple ferromagnetically, and hence such polymers exhibit RT-FM. Furthermore, cooling stretched Teflon tape promoted the FM, since the dynamic motion of the polymer chains was suppressed. Moreover, magnetic anisotropy with the easy axis perpendicular to the cut edges was observed in both the cut Teflon and Parafilm.

V. SUGGESTION

- Other types of polymers may be tested for simple deformation and RT-FM to establish a strong evidence to support the assumption.
- RT-FM in thin film polymers is of interest in terms of application point of view.

VI. REFERENCES

Andriotis A N, Menon M, Sheetz R M and Chernozatonskii L (2003), "Magnetic properties of C-60 polymers," *Phys. Rev. Lett.*, vol. 90, pp. 026801 Artn 026801,Doi 10.1103/Physrevlett.90.026801.

Bunn C W and Howells E R (1954), "Structures of molecules and crystals of fluorocarbons," *Nature*, vol. 174, pp. 549-551.

Esquinazi P, Setzer A, Hohne R, Semmelhack C, Kopelevich Y, Spemann D, Butz T, Kohlstrunk B and Losche M (2002), "Ferromagnetism in oriented graphite samples," *Phys. Rev. B*, vol. 66, pp. 024429 Artn 024429, Doi 10.1103/Physrevb.66.024429.

Esquinazi P, Spemann D, Hohne R, Setzer A, Han K H and Butz T (2003), "Induced magnetic ordering by proton irradiation in graphite," *Phys. Rev. Lett.*, vol. 91, pp. 227201 Artn 227201, Doi 10.1103/Physrevlett.91.227201.

Friedman A L, Chun H, Jung Y J, Heiman D, Glaser E R and Menon L (2010), "Possible room-temperature ferromagnetism in hydrogenated carbon nanotubes," *Phys. Rev. B*, vol. 81, pp. 115461 Artn 115461, Doi 10.1103/Physrevb.81.115461.

Han K H, Spemann D, Hohne R, Setzer A, Makarova T, Esquinazi P and Butz T (2003), "Observation of intrinsic magnetic domains in C-60 polymer," *Carbon*, vol. 41, pp. 785-795 Doi 10.1016/S0008-6223(02)00401-3.

Jain R, Kabir K, Gilroy J B, Mitchell K A R, Wong K C and Hicks R G (2007), "High-temperature metal-organic magnets," *Nature*, vol. 445, pp. 291-294 Doi 10.1038/Nature05439.

Kaburagi Y and Hishiyama Y (2002), "Ferromagnetism discovered on heat-treating the aromatic polyimide film Kapton," *J. Mater. Res.*, vol. 17, pp. 2000-2006 Doi 10.1557/Jmr.2002.0296.

Lehtinen P O, Foster A S, Ma Y C, Krasheninnikov A V and Nieminen R M (2004), "Irradiation-induced magnetism in graphite: A density functional study," *Phys. Rev. Lett.*, vol. 93, pp. 187202 Artn 187202, Doi 10.1103/Physrevlett.93.187202.

Ma Y W, Lu Y H, Yi J B, Feng Y P, Herng T S, Liu X, Gao D Q, Xue D S, Xue J M, Ouyang J Y and Ding J (2012), "Room temperature ferromagnetism in Teflon due to carbon dangling bonds," *Nat Commun*, vol. 3, pp. 727 http://www.nature.com/ncomms/journal/v3/n3/suppinfo/ncomms1689_S1.html.

Manriquez J M, Yee G T, McLean R S, Epstein A J and Miller J S (1991), "A Room-Temperature Molecular/Organic-Based Magnet," *Science*, vol. 252, pp. 1414-1417.

Miller J S and Epstein A J (2000), "Molecule-Based Magnets - An Overview," *MRS Bull.*, vol. 25, pp. 21-30.

Rajca A, Wongsriratanakul J and Rajca S (2001), "Magnetic ordering in an organic polymer," *Science*, vol. 294, pp. 1503-1505 DOI 10.1126/science.1065477.

Talapatra S, Ganesan P G, Kim T, Vajtai R, Huang M, Shima M, Ramanath G, Srivastava D, Deevi S C and Ajayan P M (2005), "Irradiation-induced magnetism in carbon nanostructures," *Phys. Rev. Lett.*, vol. 95, pp. 097201 Artn 097201, Doi 10.1103/Physrevlett.95.097201.

Veciana J and Iwamura H (2000), "Organic Magnets," *MRS Bull.*, vol. 25, pp. 41-51.

Wood R A, Lewis M H, Lees M R, Bennington S M, Cain M G and Kitamura N (2002), "Ferromagnetic fullerene," *J Phys-Condens Mat*, vol. 14, pp. L385-L391 Pii S0953-8984(02)36363-X, Doi 10.1088/0953-8984/14/22/101.

Xia H H, Li W F, Song Y, Yang X M, Liu X D, Zhao M W, Xia Y Y, Song C, Wang T W, Zhu D Z, Gong J L and Zhu Z Y (2008), "Tunable Magnetism in Carbon-Ion-Implanted Highly Oriented Pyrolytic Graphite," *Adv. Mater.*, vol. 20, pp. 4679-4683 DOI 10.1002/adma.200801205.

Zanolli Z and Charlier J C (2010), "Spin transport in carbon nanotubes with magnetic vacancy-defects," *Phys. Rev. B*, vol. 81, pp. 165406 Artn 165406, Doi 10.1103/Physrevb.81.165406.

Output ที่ได้จากโครงการวิจัย

1. ผลงานตีพิมพ์ในวารสารวิชาการนานาชาติ (ระบุชื่อผู้แต่ง ชื่อเรื่อง ชื่อวารสาร ปี เล่มที่ เลขที่ และหน้า) หรือผลงานตามที่คาดไว้ในสัญญาโครงการ ประกอบไปด้วย

   - Nipaporn Sriplai, Supree Pinitsoontorn*, Apiwat Chompoosor, Sittipong Amnuaypanich, Santi Maensiri, Vittaya Amornkitbamrung, “Ferromagnetism in Metal-Free Polymers”, *IEEE Magnetics Letters* **6**, 1000104 (2015).

   - Pornjuk Srepusharawoot, Supree Pinitsoontorn*, Santi Maensiri, “Electronic structure of iron-doped misfit-layered calcium cobaltite”, *Computational Materials Science* **114**, 64-71 (2016).

2. การนำผลงานวิจัยไปใช้ประโยชน์

   - มีการพัฒนาการเรียนการสอนในหลักสูตรวัสดุศาสตร์และนาโนเทคโนโลยี ในรายวิชา 301340 วัสดุแม่เหล็ก สำหรับนักศึกษาระดับปริญญาตรี และในรายวิชา 301706 วัสดุแม่เหล็ก สำหรับนักศึกษาระดับบัณฑิตศึกษา

3. การเสนอผลงานในที่ประชุมวิชาการ

   - Supree Pinitsoontorn, “Room temperature ferromagnetism observation in metal-free polymers”, *The 2nd Annual Meeting on Advanced Functional Materials (AFM-II)*, at Suranaree University of Technology, Nakhon Ratchasima, Thailand, on 7 August 2015 (invited talk).

ภาคผนวก

Reprint ของผลงานตีพิมพ์ทั้ง 2 ฉบับ

Nipaporn Sriplai, Supree Pinitsoontorn*, Apiwat Chompoosor, Sittipong Amnuaypanich, Santi Maensiri, Vittaya Amornkitbamrung, “Ferromagnetism in Metal-Free Polymers”, *IEEE Magnetics Letters* **6**, 1000104 (2015).

Pornjuk Srepusharawoot, Supree Pinitsoontorn*, Santi Maensiri, “Electronic structure of iron-doped misfit-layered calcium cobaltite”, *Computational Materials Science* **114**, 64-71 (2016).

Magnetism in Solids

Ferromagnetism in Metal-Free Polymers

Nipaporn Sriplai[1], Supree Pinitsoontorn[1,2], Apiwat Chompoosor[1,2], Sittipong Amnuaypanich[3], Santi Maensiri[4], and Vittaya Amornkitbamrung[2]

[1]*Materials Science and Nanotechnology Program, Faculty of Science, Khon Kaen University, Khon Kaen 40002, Thailand*
[2]*Integrated Nanotechnology Research Center, Department of Physics, Faculty of Science, Khon Kaen University, Khon Kaen 40002, Thailand*
[3]*Department of Chemistry, Faculty of Science, Khon Kaen University, Khon Kaen 40002, Thailand*
[4]*School of Physics, Institute of Science, Suranaree University of Technology, Nakhon Ratchasima 30000, Thailand*

Received 14 Apr 2015, revised 30 Apr 2015, accepted 11 May 2015, published 1 Jun 2015, current version 26 Aug 2015.

Abstract— It has recently been shown that room temperature ferromagnetism (RT-FM) can be induced in Teflon by simple stretching or cutting. The question was raised whether this is a common phenomenon in any polymer. We carried out several experiments to show that RT-FM could not be induced in all polymers. We mechanically deformed several polymers, i.e., Teflon (polytetrafluoroethylene), natural rubber (polyisoprene), PVDF (polyvinylidene fluoride), PP (polypropylene), and Parafilm (polyethylene), by simply stretching or cutting. Only Teflon and Parafilm exhibited induced RT-FM, whereas other polymers showed paramagnetic behavior. It has been believed that induced RT-FM is caused by a combination of the formation of carbon dangling bonds and ferromagnetic coupling between them. Carbon dangling bonds were generated in all polymers subjected to mechanical deformation. However, ferromagnetic coupling of the carbon dangling bonds could occur only in crystalline polymers with the right chain separation distance ($\sim$5 Å), e.g., Teflon and Parafilm. In addition, magnetic anisotropy could be observed in the cut Teflon and Parafilm. In both cases, the easy axis was in the direction perpendicular to the cut edges.

Index Terms—Magnetism in solids, polymers, ferromagnetism, room temperature, carbon dangling bond.

I. INTRODUCTION

Ferromagnetism in carbon-based materials is of particular interest for use in lightweight, flexible, and cheap magnets. These carbon-based magnets also have potential application in spintronics, since carbon may provide an easy way to integrate spin and molecular electronics [Xia 2008]. However, ferromagnetism in organic materials containing only light elements can be observed only at low temperature ($<$10 K) [Veciana 2000, Rajca 2001] and so cannot be utilized for any real application. A traditional way to induce room temperature ferromagnetism (RT-FM) in carbon materials is by incorporating metal ions into molecular/organic polymer-based materials [Manriquez 1991, Miller 2000, Jain 2007]. RT-FM in metal-free organic material was discovered in C_{60} subjected to a high-pressure and high-temperature polymerization process [Wood 2002, Han 2003]. Subsequently, RT-FM in other forms of pure carbon has been continuously reported including graphite [Esquinazi 2003, Xia 2008], carbon nanotubes [Friedman 2010], and nanosized diamonds [Talapatra 2005]. In addition, RT-FM was discovered in the aromatic polyimide film Kapton, thermally treated at temperatures between 490 and 540 °C [Kaburagi 2002]. The observed FM in these carbon-based materials was believed to be of intrinsic origin. An effect from magnetic impurities was ruled out, since no correlation between FM and the magnetic impurity concentration was found [Esquinazi 2002]. The source of FM was attributed to unpaired electrons from defects in the structure. This was also supported by *ab initio* calculations in a few different carbon systems [Andriotis 2003, Lehtinen 2004, Zanolli 2010].

In observations of RT-FM in carbon-based materials, the samples were treated by a high pressure process [Wood 2002, Han 2003], high temperature postannealing [Kaburagi 2002, Friedman 2010], or by irradiation [Esquinazi 2003, Talapatra 2005, Xia 2008]. Ma [2012] reported that RT-FM can be realized in Teflon tape (polytetrafluoroethylene) when subjected to simple stretching and cutting. The authors explained, using first-principle calculation, that the origin of FM was due to carbon dangling bonds and strong ferromagnetic coupling between them. Furthermore, RT-FM was observed in polyethylene by simply cutting the polymer in an inert atmosphere. The experimental results of Ma [2012] are of interest since they open up an easy and inexpensive option for creating FM in metal-free polymers. The question now is if these techniques are applicable to other types of polymers. This point is the objective of our study. Hence, in this paper, we investigated RT-FM in different polymers, i.e., Teflon tape, natural rubber (polyisoprene), PP (polypropylene), PVDF (polyvinylidene fluoride) and Parafilm (polyethylene). They were subjected to mechanical deformation and magnetic measurements were carried out.

II. EXPERIMENTS

Five different types of polymers that are easily obtained or commonly used in the lab were selected as the subjects of the experiments. Samples of Teflon tape, Parafilm, and PP were purchased whereas natural rubber was prepared by drying commercial latex. PVDF was prepared by the polymerization of the monomer in dimethylformamide (DMF) and drying at

Corresponding author: S. Pinitsoontorn (psupree@kku.ac.th).
This paper has supplementary downloadable material available at http://ieeexplore.ieee.org provided by the authors. The material is 5 MB.
Digital Object Identifier 10.1109/LMAG.2015.2437971

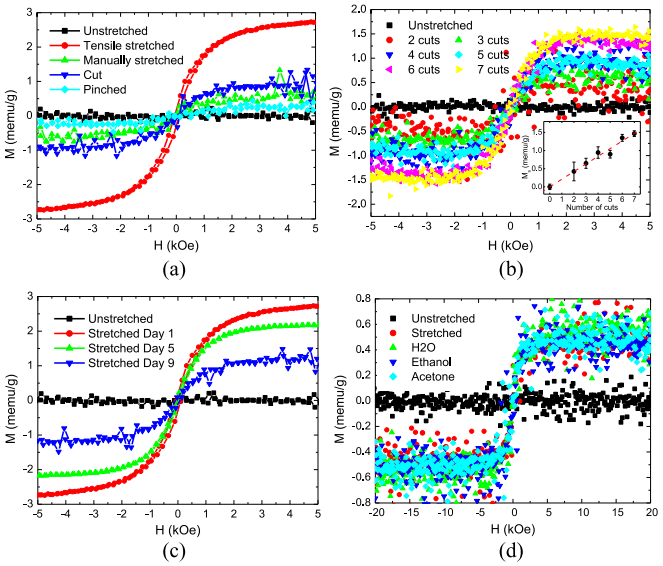

Fig. 1. Room temperature *M–H* curves of (a) Teflon subjected to several mechanical deformations. (b) Teflon tape as a function of number of cuts (inset shows saturation magnetization (M_s) versus the number of cuts), (c) tensile-stretched Teflon after being left in a normal atmosphere, and (d) stretched Teflon after being submerged in different solutions. In every curve, the diamagnetic signals were subtracted from the raw data.

60 °C. Fourier transform infrared spectroscopy (FTIR, Bruker, Tensor27) was used to confirm the functional group of each polymer. To perform the experiment on RT-FM by mechanical deformation, all polymers were cut to have a weight of around 20–40 mg with a length of 30–60 mm and width of 10–18 mm. To avoid any contamination, the samples were carefully handled and a ceramic knife was used for cutting. The polymers were then subjected to mechanical deformation by several means, i.e., simple stretching using a universal testing machine (UTM, Instron 5567A) or by hand, or cutting into several pieces, or pinching with a nonmagnetic needle. The samples were mounted onto a quartz rod for the magnetic measurements. Details with illustrations of sample preparation and manipulation can be found in the supplementary information. The magnetization of the samples at room temperature before and after mechanical deformation was measured using a vibrating sample magnetometer option in the Quantum Design VersaLab Instrument, USA. To obtain information on the crystallinity of each polymer, samples were characterized using X-ray diffraction (XRD) with an X-ray diffractometer employing Cu Kα radiation (Bruker, D2 PHASER). Furthermore, all polymers were subjected to elemental analysis using energy-dispersive X-ray spectroscopy (EDS) equipped on the scanning electron microscope (SEM, SEC SNE-4500M). In addition, electron spin resonance (ESR) spectra for inspection of unpaired electrons were obtained using an ESR spectrometer (JEOL, JES-RE2X).

III. RESULTS AND DISCUSSION

We started our experiment by investigating RT-FM in Teflon tape, similarly to the experiments of Ma [2012]. The result of the *M–H* curve measurement of the as-prepared unstretched Teflon tape was a typical diamagnetic characteristic. The RT-FM of Teflon tape was induced by simply stretching by hand. The result at this point resembled the work done by Ma [2012]. According to Ma [2012], the observed RT-FM can be attributed to carbon dangling bonds and their ferromagnetic coupling.

We further investigated whether other types of mechanical deformation could affect the RT-FM of the Teflon tape. The results are shown in Fig. 1(a), which demonstrates the *M–H* loops of the Teflon tape subjected to many kinds of deformations. RT-FM of the mechanically deformed Teflon tape can be found in all treatments. The strongest ferromagnetic signal was found in Teflon tape subjected to tensile stretching using the universal testing machine (UTM). This is because the UTM can uniformly stretch the sample and possibly generate a larger number of dangling bonds compared to the other methods. In fact, the magnetization value in our case is much greater than that reported by Ma [2012]. This may be due to the severe deformation of the Teflon tape by tensile stretching in our case (see the image in the supplementary information), which probably creates more dangling bonds. The samples cut into small pieces also show the RT-FM signal [see Fig. 1(b)]. The inset of Fig. 1(b) shows the variation of saturation magnetization (M_s) as a function of the number of cuts. Pinching the samples with a nonmagnetic needle can induce RT-FM, but the signal is much smaller than for the stretched or cut samples. The easiest method in producing RT-FM in Teflon is by simply stretching the sample by hand [manually stretched in Fig. 1(b)]. Since this is the simplest method, the RT-FM in polymers in the following texts is induced by manually stretching, unless stated otherwise. In all cases, the coercivity is very low ($<$ 100 Oe). Note that the *M–H* curves in Fig. 1 were processed by removing the diamagnetic signals. The slope of the diamagnetic part was calculated and used for background subtraction. After removing the diamagnetic signals, only the FM signals were observed for the mechanically deformed samples and a flat curve near zero was observed for the unstretched sample.

The stability of the RT-FM of the stretched Teflon tape was tested by measuring the magnetic properties after exposing the tensile-stretched samples to normal atmosphere for several days. The results are presented in Fig. 1(c). It can be seen that the magnetization gradually decreased from day one to day nine. As was mentioned that the origin of FM in Teflon is due to the carbon dangling bonds, these dangling bonds may not be stable in normal atmosphere. It is possible that oxygen or water molecules (due to the high humidity in Thailand) may be absorbed and saturate the dangling bonds, eliminating FM [Ma 2012]. Next, we tested the stability of RT-FM under the influence of different solutions. We submerged the stretched Teflon in water, ethanol, or acetone and measured the *M–H* curves as shown in Fig. 1(d). It can be seen that the solution did not affect the magnetization, which may be due to the low permeability of these solutions in Teflon. Therefore, the dangling bonds were untouched and the RT-FM was unchanged.

After the FM observation in Teflon, we moved to the investigation of other polymers. The FTIR spectrum of each sample was obtained to confirm the functional groups of the polymers used in this study. The FTIR results are available in the supplementary information. Fig. 2 shows the *M–H* curves of the

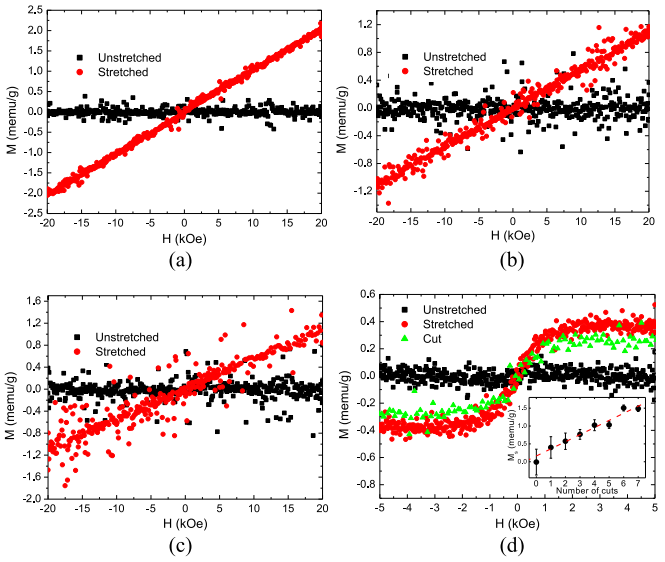

Fig. 2. Room temperature *M–H* curves of several polymers subjected to simple stretching or cutting: (a) Natural rubber. (b) PVDF. (c) PP. (d) Parafilm, inset shows saturation magnetization (M_s) versus the number of cuts. In every curve, the diamagnetic signals were subtracted from the raw data.

investigated polymers after diamagnetic signal subtraction. For natural rubber, PP and PVDF, RT-FM was not observed. PVDF was chosen because the chain structure of PVDF $(\text{-CF}_2\text{-CH}_2\text{-})_n$ is similar to Teflon $(\text{-CF}_2\text{-CF}_2\text{-})_n$. The absence of RT-FM in PVDF indicates that the ferromagnetic behavior is irrelevant to the C-F bonds or their related interaction. However, Fig. 2 shows the change in the slopes of the graph for the stretched natural rubber, PP, and PVDF, compared to the unstretched samples. The positive slopes of the *M–H* curves indicate paramagnetism. From these results, it can be interpreted that stretching the natural rubber, PP, and PVDF results in the formation of carbon dangling bonds as a source of available magnetic moments ($1\mu_B$ per 1 dangling bond). However, the lack of ferromagnetic coupling of these dangling bonds suppresses the RT-FM in such polymers. On the other hand, Fig. 2(d) shows the *M–H* curves of the unstretched, stretched, and cut Parafilm. It is obvious that stretching or cutting Parafilm results in the characteristic S-shape curves of ferromagnetic materials. The inset of Fig. 2(d) shows the variation of saturation magnetization (M_s) as a function of the number of cuts. The origin of the RT-FM in Parafilm is also attributable to the ferromagnetic coupling of carbon dangling bonds. This part of our experiment shows that RT-FM is not observed in all polymers by simply stretching or cutting. Only some polymers exhibit this behavior, i.e., Teflon and Parafilm. Hence, there must be other influential factors for inducing RT-FM.

To answer the question, the XRD patterns of the unstretched polymers used in the experiment were measured as shown in supplementary information. The XRD patterns of the unstretched and stretched polymers were found to be insignificantly different. The XRD pattern of the Teflon sample can be matched with JCPDS card (47–2217), corresponding to the pseudohexagonal structure with $a = b = 5.66$ Å, similar to a previous report [Bunn 1954]. The very sharp peak at $2\theta = 18.10^\circ$ indicates the high crystallinity of the sample. For natural rubber and PVDF, broad XRD spectra were observed, implying mostly an amorphous structure. One of the reasons that RT-FM was not found in natural rubber or PVDF may be due to the absence of crystallinity. For PP and Parafilm, crystalline peaks can be observed on the amorphous background in both samples. If the crystalline structure of polymers is the reason for ferromagnetic coupling, both samples should exhibit ferromagnetic behavior. However, RT-FM was only observed in Parafilm but not PP. The crystalline part of the PP sample can be matched with the JCPDS card (50–2397) corresponding to the monoclinic structure with the lattice parameters of $a = 6.63$ Å, $b = 20.78$ Å and $c = 6.50$ Å. The XRD pattern of Parafilm can be related to the orthorhombic polyethylene structure with $a = 7.40$ Å, $b = 4.93$ Å and $c = 2.54$ Å, JCPDS card (53–1859). Ma [2012] used the first principle calculation to show that the ferromagnetic coupling is energetically favorable only when the chain separation is around 5 Å. Our XRD results show that only Teflon and Parafilm fall in this criterion, which leads to ferromagnetic coupling of carbon dangling bonds after stretching or cutting.

To ensure that the ferromagnetic signals of Teflon and Parafilm are from the intrinsic origin, energy dispersive X-ray spectra of the unstretched and stretched samples were measured. The metallic impurity was not found in all the spectra (supplementary information). The detection limit of the EDS is typically about 1000 ppm by weight. Therefore, using the EDS alone may not be able to distinguish FM from impurity sources. However, we are still confident that the origin of RT-FM in the particular polymers is intrinsic. Several reasons support this argument. First, the difference in magnetic behavior before and after stretching Teflon (and Parafilm), using the same piece of sample, can be clearly observed. Second, the saturation magnetization values of Teflon [see Fig. 1(b)] and Parafilm [see Fig. 2(d)] increase as a function of number of cuts, indicating that the larger number of dangling bonds can directly affect the FM behavior. Finally, the magnetization of the stretched Teflon decreases with time [see Fig. 1(c)]. The combination of all this evidence can effectively reject the existence of metallic impurities and verify the intrinsic origin of the RT-FM.

In this paper, we have shown that by simple stretching or cutting or other form of mechanical deformation, the RT-FM of Teflon and Parafilm can be created. However, this RT-FM cannot be generated for any polymer in general. We suggest a guideline for observing RT-FM in polymers as follows. 1) The polymer must be mostly crystalline. Stretching or cutting amorphous polymers can result in the formation of isolated dangling bonds without any magnetic interaction. This would thus induce only paramagnetism. 2) The separation between the chains of the polymer must be at the right distance (around 5 Å). A smaller distance results in antiferromagnetic coupling, whereas for further separation, no magnetic exchange coupling exists.

The ESR spectra (first derivative) of each polymer are shown in Fig. 3. ESR spectroscopy is a technique for studying materials with unpaired electrons. At the right combination of frequency and magnetic field values, the unpaired electrons can switch between their two spin states (the lower and upper states). Hence, ESR spectra can be used to detect the existence of

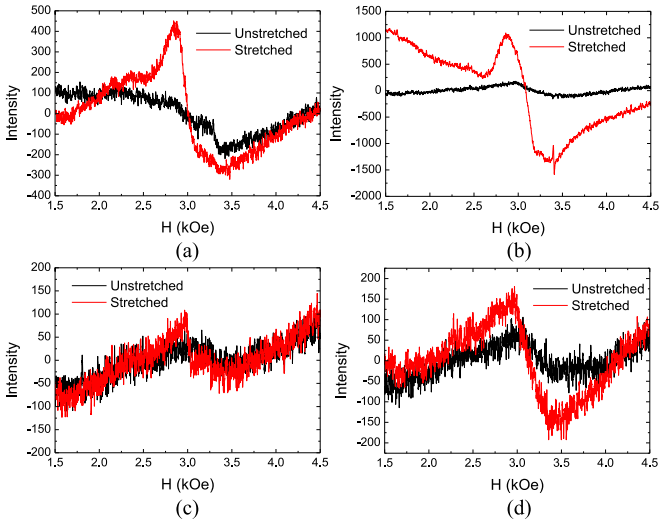

Fig. 3. Comparison of ESR spectra between unstretched and stretched polymers: (a) Teflon. (b) Natural rubber. (c) PVDF. (d) Parafilm.

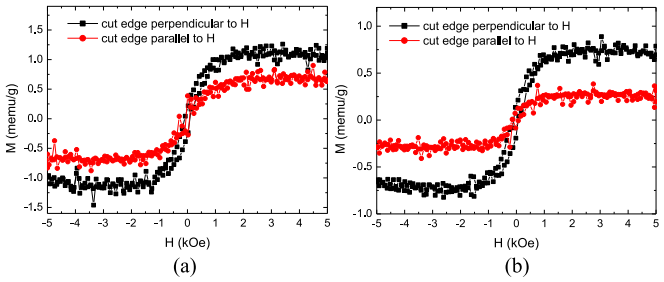

Fig. 4. Magnetic anisotropic behavior of (a) Teflon and (b) Parafilm when the applied field is perpendicular or parallel to the cut edge.

unpaired electrons in the materials. The intensity of the signal depends on the concentration of the unpaired electrons. From Fig. 3, it is clearly seen that the strongest change in the ESR spectra occurs between unstretched and stretched natural rubber. However, natural rubber does not exhibit RT-FM due to its lack of crystallinity. The smallest signals are observed from PVDF and PP (PP signal is not shown here but very similar to PVDF signal), and the signals are nearly unchanged between the stretching states. This is the reason we do not observe RT-FM in these polymers. As discussed earlier, RT-FM can be induced in stretched Teflon and Parafilm due to the formation of carbon dangling bonds; ESR results show strong evidence to support this. Teflon and Parafilm show changes in ESR signals between stretching states, indicating the creation of dangling bonds in the stretched state. In combination with their crystallinity, RT-FM can be induced in these polymers. It should be noted that ESR signals can always be found in unstretched polymer. This is because very small pieces of polymers are needed in the test tube for the ESR measurement. Cutting polymer into small pieces always creates some dangling bonds, which could be the source of the ESR signals.

In addition, from the above discussion, the created dangling bonds and their magnetic interactions could be dependent on the magnetic field direction; in other words, magnetic anisotropy could be observed. To test this assumption, we prepared the Teflon tapes (and Parafilm) cut into several small pieces. In one set, the samples were aligned such that their cut edges were perpendicular to the magnetic field. In the other set, the cut edges of the samples were parallel to the field. The results are shown in Fig. 4. It is obvious that an anisotropic effect can be observed. In both Teflon and Parafilm cases, the samples that had their cut edges aligned perpendicularly to the field exhibited higher magnetization, indicating that the easy axis is in the direction perpendicular to the cut edges.

ACKNOWLEDGMENT

This work was supported by the Thailand Research Fund (TRF) in cooperation with the Commission on Higher Education and Khon Kaen University under Grant MRG5680159 and the TRF Senior Research Scholar under Grant RTA5680008.

REFERENCES

Andriotis A N, Menon M, Sheetz R M, Chernozatonskii L (2003), "Magnetic properties of C_{60} polymers," *Phys. Rev. Lett.*, vol. 90, 026801, doi: 10.1103/Physrevlett.90.026801.

Bunn C W, Howells E R (1954), "Structures of molecules and crystals of fluorocarbons," *Nature*, vol. 174, pp. 549–551, doi: 10.1038/174549a0.

Esquinazi P, Setzer A, Höhne R, Semmelhack C, Kopelevich Y, Spemann D, Butz T, Kohlstrunk B, Lösche M (2002), "Ferromagnetism in oriented graphite samples," *Phys. Rev. B*, vol. 66, 024429, doi: 10.1103/Physrevb.66.024429.

Esquinazi P, Spemann D, Höhne R, Setzer A, Han K-H, Butz T (2003), "Induced magnetic ordering by proton irradiation in graphite," *Phys. Rev. Lett.*, vol. 91, 227201, doi: 10.1103/Physrevlett.91.227201.

Friedman A L, Chun H, Jung Y J, Heiman D, Glaser E R, Menon L (2010), "Possible room-temperature ferromagnetism in hydrogenated carbon nanotubes," *Phys. Rev. B*, vol. 81,115461, doi: 10.1103/Physrevb.81.115461.

Han K-H, Spemann D, Höhne R, Setzer A, Makarova T, Esquinazi P, Butz T (2003), "Observation of intrinsic magnetic domains in C_{60} polymer," *Carbon*, vol. 41, pp. 785–795, doi: 10.1016/S0008-6223(02)00401-3.

Jain R, Kabir K, Gilroy J B, Mitchell K A R, Wong K-C, Hicks R G (2007), "High-temperature metal-organic magnets," *Nature*, vol. 445, pp. 291–294, doi: 10.1038/Nature05439.

Kaburagi Y, Hishiyama Y (2002), "Ferromagnetism discovered on heat-treating the aromatic polyimide film Kapton," *J. Mater. Res.*, vol. 17, pp. 2000–2006, doi: 10.1557/Jmr.2002.0296.

Lehtinen P O, Foster A S, Ma Y C, Krasheninnikov A V, Nieminen R M (2004), "Irradiation-induced magnetism in graphite: A density functional study," *Phys. Rev. Lett.*, vol. 93, 187202, doi: 10.1103/Physrevlett.93.187202.

Ma Y W, Lu Y H, Yi J B, Feng Y P, Herng T S, Liu X, Gao D Q, Xue D S, Xue J M, Ouyang J Y, Ding J (2012), "Room temperature ferromagnetism in Teflon due to carbon dangling bonds," *Nature Commun.*, vol. 3, 727, doi: 10.1038/ncomms1689.

Manriquez J M, Yee G T, McLean R S, Epstein A J, Miller J S (1991), "A room-temperature molecular/organic-based magnet," *Science*, vol. 252, pp. 1414–1417, doi: 10.1126/science.252.5011.1415.

Miller J S, Epstein A J (2000), "Molecule-based magnets—An overview," *MRS Bull.*, vol. 25, pp. 21–30, doi: 10.1557/mrs2000.221.

Rajca A, Wongsriratanakul J, Rajca S (2001), "Magnetic ordering in an organic polymer," *Science*, vol. 294, pp. 1503–1505, doi: 10.1126/science.1065477.

Talapatra S, Ganesan P G, Kim T, Vajtai R, Huang M, Shima M, Ramanath G, Srivastava D, Deevi S C, Ajayan P M (2005), "Irradiation-induced magnetism in carbon nanostructures," *Phys. Rev. Lett.*, vol. 95, 097201, doi: 10.1103/Physrevlett.95.097201.

Veciana J, Iwamura H (2000), "Organic magnets," *MRS Bull.*, vol. 25, pp. 41–51, doi: 10.1557/mrs2000.23.

Wood R A, Lewis M H, Lees M R, Bennington S M, Cain M G, Kitamura N (2002), "Ferromagnetic fullerene," *J Phys., Condens. Matter*, vol. 14, pp. L385–L391, doi: 10.1088/0953-8984/14/22/101.

Xia H H, Li W F, Song Y, Yang X M, Liu X D, Zhao M W, Xia Y Y, Song C, Wang T-W, Zhu D Z, Gong J L, Zhu Z Y (2008), "Tunable magnetism in carbon-ion-implanted highly oriented pyrolytic graphite," *Adv. Mater.*, vol. 20, pp. 4679–4683, doi: 10.1002/adma.200801205.

Zanolli Z, Charlier J-C (2010), "Spin transport in carbon nanotubes with magnetic vacancy-defects," *Phys. Rev. B*, vol. 81, 165406, doi: 10.1103/Physrevb.81.165406.

Computational Materials Science 114 (2016) 64–71

Contents lists available at ScienceDirect

Computational Materials Science

journal homepage: www.elsevier.com/locate/commatsci

Electronic structure of iron-doped misfit-layered calcium cobaltite

Pornjuk Srepusharawoot [a,b], Supree Pinitsoontorn [a,b,*], Santi Maensiri [c]

[a] Department of Physics, Faculty of Science, Khon Kaen University, Khon Kaen 40002, Thailand
[b] Integrated Nanotechnology Research Center, Khon Kaen University, Khon Kaen 40002, Thailand
[c] School of Physics, Institute of Science, Suranaree University of Technology, Nakhon Ratchasima 30000, Thailand

ARTICLE INFO

Article history:
Received 12 June 2015
Received in revised form 30 October 2015
Accepted 7 December 2015

Keywords:
$Ca_3Co_4O_9$
Thermoelectric oxide
Transition metal doping
Electronic structure
Thermopower

ABSTRACT

The electronic structures of the undoped and Fe-doped misfit-layered calcium cobaltite are calculated using the first-principles calculations under DFT + U scheme. The calculated density of states (DOS) of the undoped sample is in a good agreement with the past theoretical calculation and experiments. The Fermi level falls at nearly the top of the valence band of the CoO_2 sublattice. The obtained magnetization could also very well explain the previous experiments. With Fe doping, two obvious changes in the DOS can be observed. Firstly, the Fermi energy has shifted to the higher level value and intercepted at the edge of the valence band where the slope is maximum. This characteristic enhances the thermopower of the system. The second change is the additional states ~0.1 eV above the Fermi level coming from the states of Fe atoms. These states are interpreted as a source of charge reservoir providing holes for electrical conduction in the CoO_2 layer. The electronic structures of the Fe-doped case show very good agreement with the previous thermoelectric measurements. The thermopower, calculated using Boltzmann transport theory, is significantly enhanced in the Fe-doped system compared to the undoped one.

1. Introduction

Thermoelectric materials can directly convert heat into electricity. Good thermoelectric materials should possess high electrical conductivity (σ), low thermal conductivity (κ) and large Seebeck coefficient (thermopower, S). Thermopower is the ratio between the generated voltage at both ends of the sample (ΔV) and the applied the temperature difference (ΔT), i.e. $S = \Delta V/\Delta T$. A dimensionless figure-of-merit (ZT), defined as $ZT = S^2\sigma T/\kappa$, is generally used to determine the efficiency of any thermoelectric material. Conventionally, such properties are optimized in intermetallic compounds, e.g. Bi_2Te_3, PbTe or SiGe [1]. Oxide materials have been extensively researched as potential materials for thermoelectric applications in recent years since a discovery of a large thermopower in $NaCo_2O_4$ single crystals [2]. Amongst p-type thermoelectric oxide, calcium cobaltite ($Ca_3Co_4O_9$) is one of the most promising thermoelectric materials. It possesses a combination of relatively high σ and S and low κ, with ZT comparable to conventional materials [3]. Moreover, this material exhibits a number of interesting properties such as strongly correlated properties [4], anisotropic magnetic properties [5,6], unconventional Hall effect [7], or even giant dielectric behaviour [8]. A number of structural investigations of this material have been conducted [9–12]. It has been shown that $Ca_3Co_4O_9$ is in fact a simplification of the actual composition of $[Ca_2CoO_3]_n[CoO_2]$, where n is close to the golden ratio (1.618). Its structure consists of two sublattices: a rocksalt (RS)-type Ca_2CoO_3 layer and a CdI_2-type CoO_2 layer, stacking alternatively along the c axis. The lattice parameters in the a and c directions for both layers are equal but are incommensurate in the b direction.

Transport properties of $Ca_3Co_4O_9$ (CCO) were reported to be highly anisotropic with the ab-plane σ and S much larger than those in the c-axis direction [5,13]. Such experimental results are believed to be a result of the in-plane conduction of the CoO_2 layer which was confirmed by the XPS study [14]. In spite of a number of successful experiments to explain transport and thermoelectric properties of CCO, very few computational calculations have been carried out. For electronic structure calculation, there have been only the works done by Asahi et al. [15], Rebola et al. [16] and Tang et al. [13]. Asahi et al. carried out the first-principles calculations of CCO using density functional theory (DFT) and presented the densities of states (DOS) and the band structure [15]. They also estimated the thermopower from their calculation using the modified Heikes formula [17]. However, their calculation contradicted the experimental results because they showed that the thermopower and transport properties are the contribution from the RS layer. Rebola

* Corresponding author at: Department of Physics, Faculty of Science, Khon Kaen University, Khon Kaen 40002, Thailand.
E-mail address: psupree@kku.ac.th (S. Pinitsoontorn).

http://dx.doi.org/10.1016/j.commatsci.2015.12.006
0927-0256/

et al. solved this problem by using DFT + U formalism in their calculation to account for the highly correlated properties of CCO [16]. Their results showed that with DFT + U the DOS has been modified such that the electron contribution near Fermi level was mostly limited to the CoO_2 layer, in an agreement with the experiment [14]. On the other hand, Tang et al. calculated the band structure of CCO and explained the anisotropic *S* as a difference in Fermi surface in each direction [13].

For thermoelectric application, it is important to maximize *ZT* of thermoelectric materials. One way to increase the *ZT* of CCO is to dope it with other elements. Partial substitution of Co with other transition metals has been employed to improve thermoelectric properties [18–26]. Particularly, experimental results showed that the thermoelectric properties of CCO doped with Fe (CCO–Fe) were significantly improved [22,23,27]. Unlike other elemental doping, Fe doping can enhance both σ and *S* simultaneously [22,23,27]. Up to date, there has not been any computational study for the effect of doping on the electronic structure of CCO. Hence it is interesting to investigate this CCO–Fe system from the theoretical and technological points of view. In this article, we present the results of our study on the DOS of CCO–Fe. The calculated electronic structures of both CCO and CCO–Fe are discussed in terms of the transport, thermoelectric and magnetic properties.

2. Computational methods and details

A crystal structure model of CCO was constructed starting with the data from the experimental values [10]. The lattice parameters of the monoclinic structure unit cell were $a = 4.8381$ Å, $b_1 = 4.5347$ Å, $c = 10.8558$ Å, $\beta = 98.1136°$. The misfit ratio of 1.618 between the CoO_2 layer and the RS layer makes the real unit cell too large for our computational resource. Instead, we built a relatively small unit cell with the CoO_2/Ca_2CoO_3 ratio of 5/3. The reduction of the unit cell size was justified based on the work done by Rebola et al. which showed that the 5/3 approximant was sufficient in modeling the essential electronic properties of CCO [16]. Furthermore, the aim of this work is to investigate the effect of Fe substitution for Co on the electronic structure. To limit the concentration of Fe solute atoms in our model (so that it can be compared with experimental data) the unit cell size of CCO was double in the *a* direction. In other words, the formula of our model crystal structure of CCO can be written as $Ca_{24}Co_{32}O_{76}$ or $[Ca_2CoO_3]_{12}[CoO_2]_{20}$ as shown in Fig. 1.

To investigate the ground state crystal structures, the spin polarized density functional theory embedded in the Vienna Ab initio Simulation Package (VASP) [28] was carried out. Moreover, the LDA + U scheme [29,30] with $U = 5$ eV and $J = 1$ eV [16] was chosen for all calculations. All Co atoms were set in the ferromagnetic alignment. To test the ground state of the magnetic moment of Co atoms, the initial magnetic moment of Co was set to be 1.3 or 4.0 μ_B. With the Projector Augmented Wave (PAW) approach [31], the valence states for all potentials we used were 3s, 3p and 4s for Ca, 3d and 4s for Co, 3p, 3d and 4s for Fe, and 2s and 2p for O. The 500 eV of energy cutoff and $12 \times 4 \times 6$ of **k**-points generated by the Monkhorst–Pack scheme were employed for both relax and static calculations [32]. During structural relaxation process, the conjugate-gradient algorithm was employed to determine the ground state configuration. Force acting on each ion was calculated by the Hellmann-Feynman theorem.

To determine the electronic structure of the Fe-doped CCO, we replaced one Co atom in the RS layer with an Fe atom. In fact, there are two Co sites in the CCO system, in RS or CoO_2. Our previous works have shown that Fe atoms are preferential to stay in the RS site [20,33]. This was also confirmed by the other research group [34]. Thus, we built the model crystal structure of CCO–Fe as $Ca_{24}Co_{31}Fe_1O_{76}$ or $[Ca_2Co_{0.917}Fe_{0.083}O_3]_{12}[CoO_2]_{20}$ (Fig. 1). After Fe substitution, we re-optimized the structure using the same procedure. In order to compare the electronic structure of the CCO and CCO–Fe systems, the same values of *U* and *J* (5 and 1 eV, respectively) for the Fe atom were selected. To investigate the most preferable spin configuration of Fe, the initial magnetic moments of Fe were set as 1.3 or 4.0 μ_B. In the present work, the BoltzTraP code based on semi-classical Boltzmann transport theory was used for determining the thermoelectric properties of the CCO and CCO–Fe systems.

3. Results and discussion

We focus this work on the electronic structure of the CCO structure doped with Fe. In this section, we firstly present our calculation for the undoped CCO and compared with the previous investigations. Next, we present the result for the CCO–Fe. In both sections, the contribution from the electronic structure to the transport, thermoelectric and magnetic properties is discussed.

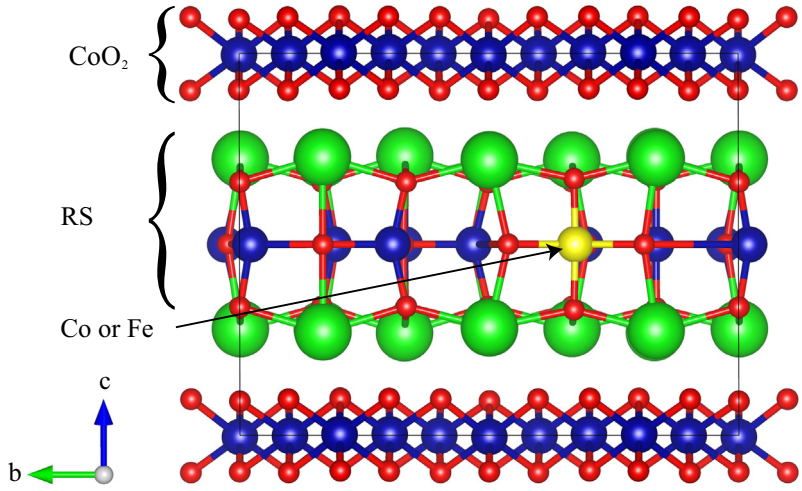

Fig. 1. The model of the unit cell of $Ca_{24}Co_{32}O_{76}$ ($[Ca_2CoO_3]_{12}[CoO_2]_{20}$) or $Ca_{24}Co_{31}Fe_1O_{76}$ ($[Ca_2Co_{0.917}Fe_{0.083}O_3]_{12}[CoO_2]_{20}$). The green, blue, and red spheres represent Ca, Co, and O atoms, respectively. The yellow sphere is either Co or Fe. (For interpretation of the references to color in this figure legend, the reader is referred to the web version of this article.)

3.1. Undoped calcium cobaltite (CCO)

The total DOS together with the partial DOS (PDOS) around the Fermi level (E_F) of the optimized CCO structure is shown in Fig. 2. It can be obviously seen that the main electronic contribution around E_F is due to a strong hybridization of O 2p and Co 3d orbitals. At Fermi level, a small but finite DOS in the spin-up channel can be found whereas there is no DOS in the spin-down channel. The mentioned features in our calculated DOS are similar to the DFT + U calculation by Rebola et al. [16] but different from the DFT calculation by Asahi et al. [15]

To investigate the transport properties from the two sublattices: RS and CoO_2, we plot the PDOS in each layer as shown in Fig. 3. One can see that the electronic structure around E_F comprises two contribution sources from both RS and CoO_2 layers. The finite PDOS of the RS layer at E_F is unexpected since the experimental result showed that the major electrical conduction is mostly limited to the CoO_2 layer [14]. However, the reason for the non-zero states in the RS layer was explained by Rebola et al. [16]. They investigated the effect of unit cell size dependence on the electronic structure. It was shown that the spin-up states at E_F in the RS layer were strongly dependent on the unit cell size. They found that using CoO_2/Ca_2CoO_3 ratio of 8/5 approximant resulted in the largest PDOS at E_F in the RS layer. In our calculation, we used the supercell which is the double size of the 5/3 approximant, making the cell size very close to the 8/5 approximant unit cell in Rebola et al. [16]. Thus, it was actually not surprised to find the states at E_F in the RS layer. Since it is really the artifact of the cell size dependence, we can neglect the spin-up states near E_F in the RS layer and reasonably assume that the electrical transport is limited to the CoO_2 layer as suggested by the experimental evidence [14].

Therefore, we focus on the DOS of CoO_2 and plot the PDOS as shown in Fig. 3. The states in the s orbital are essentially zero in both spin channels. The p and d states are found in both spin channels but at E_F only states for spin-up electrons exist. It is indicated that the contributing electrons at E_F are the p–d orbital hybridization. The Fermi level falls closely into the valley between the two peaks at −0.02 eV and +0.14 eV. Qualitatively, this would result in a relatively low σ since the maximum conductivity can be found when the E_F is located at the peak position. Furthermore, this feature in the PDOS would also suppress the thermopower. According to the semiclassical Boltzmann transport equation, the S can be calculated from [13]

$$S = \frac{\pi^2 k_B^2 T}{3e}\left[\frac{\partial \ln \sigma}{\partial E}\right]_{E=E_F} \quad (1)$$

where e and k_B are an electron charge and Boltzmann constant. The Seebeck coefficient is maximized when E_F lies close to the band edge in a narrow band where the slope of the DOS is the highest. In our calculation, the E_F is nearly at the valley between the two peaks. This characteristic is not an optimized condition for good thermoelectric properties. As can be seen in the subsequent section when doping Fe into the system, the structure of DOS has changed and leads to the improvement in the thermoelectric characteristic.

Angular momentum projections of the Co d orbitals PDOS in the CoO_2 layer are shown in Fig. 4. All spin-up and spin-down channels are fully filled in the t_{2g} bands except in the d_{xz} orbital where small empty states in the spin-up channel can be seen. In the e_g band, the spin-down states are completely filled but the spin-up states are almost completely filled. The Fermi falls nearly at the valley near the band edge of the spin-up e_g band. It is well known that the Co ions in the CoO_2 layer are a combination of Co^{3+} and Co^{4+}. The results here show that the energy of the t_{2g} and e_g bands are very similar, and both bands are a contribution from a mixture of Co^{3+} and Co^{4+} ions. Furthermore, it can be inferred that both Co^{3+} and Co^{4+} ions are in their low spin configurations. The low spin states of Co^{3+} and Co^{4+} ions were verified by using X-ray absorption [35] and X-ray photoemission [36]. Therefore, although our projections of the d states of the CoO_2 sublattice are somewhat different from the earlier simulation done by Rebola et al. [16], it can give a better picture of the electronic structure of the CoO_2 subsystem.

The calculated magnetic moments are reported in Table 1. As mentioned earlier, we set our initial configuration to be ferromagnetic for all Co atoms. As shown in Table 1, for CCO, the final

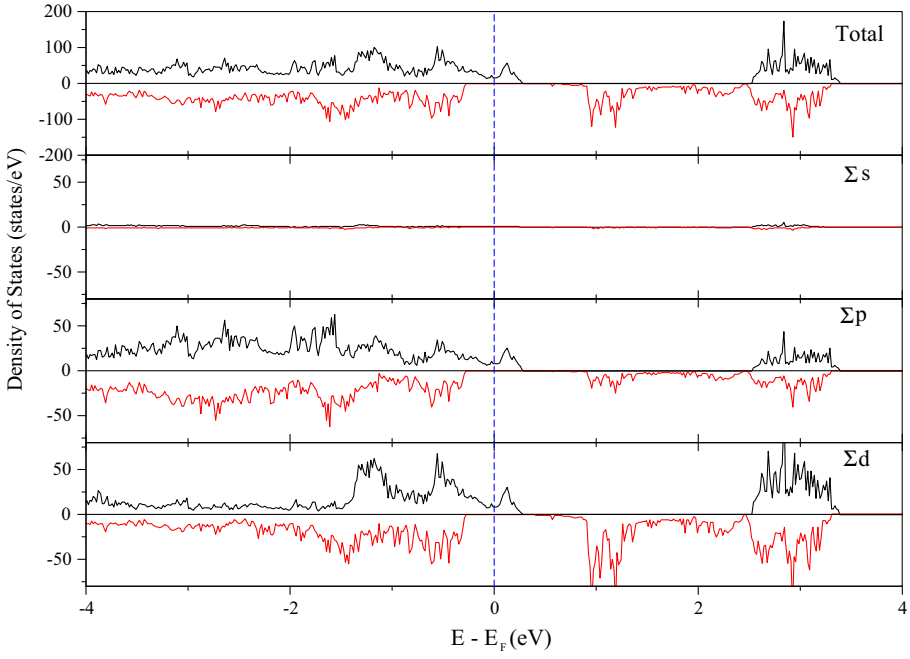

Fig. 2. Total DOS and PDOS in the sum of s, p, d orbitals of the CCO system. Black and red lines represent the spin-up and spin-down channels, respectively. The Fermi level is shown with the blue vertical dashed line. (For interpretation of the references to color in this figure legend, the reader is referred to the web version of this article.)

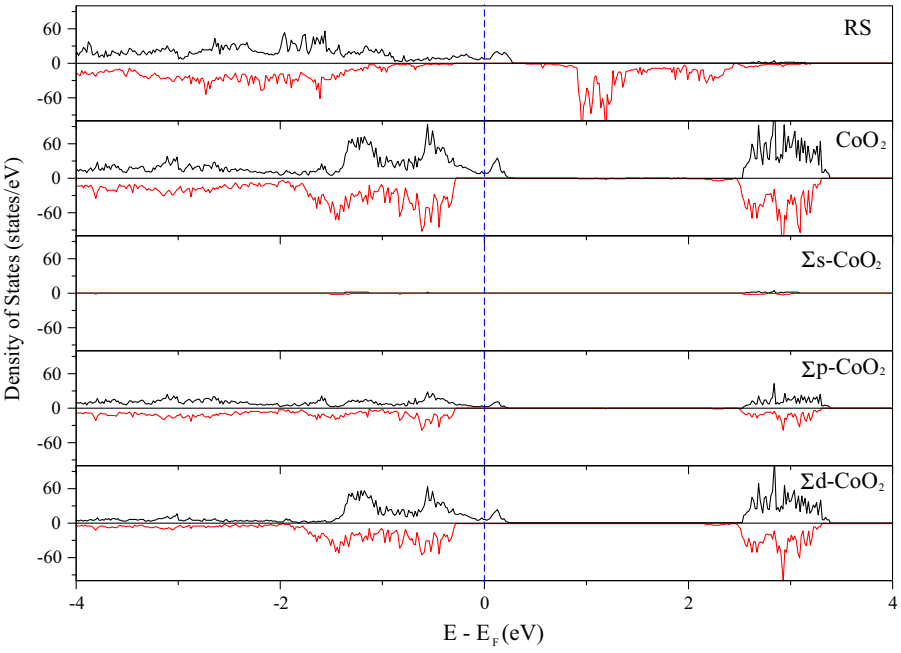

Fig. 3. PDOS of CCO in the RS and CoO_2 subsystems, and the sum of s, p, d, orbitals in the CoO_2 layer.

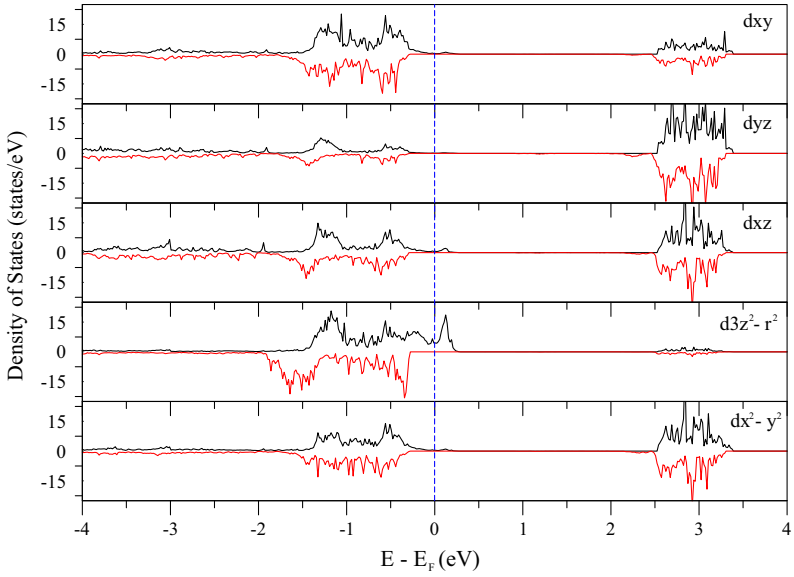

Fig. 4. PDOS projected into angular momentum resolved d orbitals in the CoO_2 layer of CCO.

Table 1
Initial magnetic moments (μ_B) of Co and Fe atoms and the averaged magnetic moments (μ_B) in the RS and CoO_2 sublattice and the total moments for the CCO and CCO–Fe systems. The relative total energies ΔE for the CCO and CCO–Fe systems having different initial magnetic moments are also included.

System	Initial moment		M_{ave}			ΔE (eV)
	Co atom	Fe atom	RS	CoO_2	Total	
CCO	1.3	–	2.75	−0.13	1.31	0.0
	4.0	–	2.78	1.10	1.94	+6.85
CCO–Fe	1.3	1.3	2.89	0.19	1.54	0.0
	1.3	4.0	2.87	0.08	1.48	+0.76

magnetic moments are significantly different when changing the initial value from 1.3 to 4.0 μ_B. The initial magnetization of 4.0 μ_B resulted in the ferromagnetic configuration both the RS and CoO_2 sublattice. On the other hand, for the initial magnetization of 1.3 μ_B, the ferromagnetism arises from the RS sublattice only whereas the moments of Co atoms in the CoO_2 are diminished. The calculated result for the initial magnetization of 1.3 μ_B is in an excellent agreement with the earlier calculation [16]. To further

confirm the interpretation, the total energy of the two systems having different initial magnetic moment (1.3 and 4.0 μ_B) was calculated. As shown in Table 1., the total energy of the system with the 1.3 μ_B is lower than the other system by 6.85 eV, indicating that this system is the ground state. The DOS and PDOS shown in Figs. 2–4 are from the 1.3 μ_B initial condition.

3.2. Fe-doped calcium cobaltite (CCO–Fe)

The total DOS and PDOS in s, p, d orbitals of CCO–Fe are presented in Fig. 5. Several features of the DOS of the Fe-doped sample do not change from the undoped sample. For instance, there are only spin-up electrons at the Fermi level; E_F falls in the band gap of the spin-down electrons. Furthermore, the conduction electrons near Fermi level are the p–d electrons hybridization from the O 2p, Co (and Fe) 3p and 3d electrons. However, doping Fe has changed a few important characteristic of the band structure. Firstly, the Fermi energy has shifted to the higher level such that now the E_F falls right at the edge of the valence band where the derivative of the DOS is maximized. As discussed earlier, this is the ideal DOS structure for a good thermoelectric material. According to Eq. (1), this characteristic would enhance the Seebeck coefficient. This is the reason of the improvement in the S for the Fe-doped CCO sample as observed in the experiments [22,23,27]. However, it should be noted that the position of E_F is very sensitive to the amount of doping, microstructure or other defects in the structure. Although our theoretical work has predicted an improvement of the thermopower for Fe doping, it is possible to observe a slightly decrease in S in the experiments due to other external factors [20].

Another important change is that in the spin-up channel above E_F, there are additional states at ~0.1 to 0.4 eV which is not presented in the CCO case. Such states are attributed to the substituted Fe atoms in the RS layer. The presence of these states has an important impact such that the band gap between the valance and conduction bands in the spin-up channel is significantly reduced from ~1.9 eV (Fig. 2) to ~0.1 eV. Although the states at E_F of CCO–Fe are nearly vanished and one would think that the electrical conductivity should be reduced, it can be argued that it may not be the case. At 0 K, it is generally accepted that there should not be electrons above the Fermi level. However, as the temperature rises, certain numbers of valence electrons gain sufficient energy to jump from the valence band to the conduction band. The electron distribution as a function of energy (E) and temperature follows the Fermi–Diract distribution:

$$f_F(E,T) = \frac{1}{1+\exp\left(\frac{E-E_F}{k_B T}\right)} \tag{2}$$

Above 0 K, the maximum f_F is 0.5 at $E = E_F$. For the case of CCO–Fe, this material is usually operated at high temperature up to 1000 K. Putting in the values of T = 1000 K and E–E_F = 0.1 eV (the band gap), the f_F value is calculated to be around 0.24 meaning that it can be over 20% of electrons in the conduction band of the CCO–Fe. As electrons jump into the conduction band, the holes are created in the valence band, contributing to the transport properties. Therefore, the discussion here demonstrates a possibility that the electrical conductivity of CCO–Fe may not be suppressed and can even be enhanced, particularly at high temperature, as demonstrated in the experiments [20,23,27]. Moreover, as mentioned earlier that the Fermi level is very sensitive to many factors, the real E_F in the experiments can vary from one sample to the other. The lower shift of the Fermi level from these variations can also contribute to the enhanced transport properties. It should be noted that the spin-down electrons cannot take part in the transport properties even though the band gap in the spin-down channel of CCO–Fe is significantly reduced compared to CCO. The band gap in the spin-down channel is still around 0.5 eV which makes the probability of only 0.3% for spin-down electron hopping from the valence band to the conduction band. It is two orders of magnitude lower than the spin-up electrons.

To further understand the effect of Fe doping on the electronic structure of the CCO–Fe, Fig. 6 shows a plot of PDOS in the CoO_2 and RS sublattices. It is obvious from the figure that the additional conduction band in the spin-up channel (~0.1 to 0.4 eV above E_F) are mostly due to the RS layer. This is because the Fe atom is substituted for the Co atom in the RS layer. The details of electronic structure in the RS sublattice are also shown in Fig. 6. It can be seen that the main contribution of the conduction band is from the p and d orbital states whereas the s orbitals are negligible. This additional spin-up conduction band is most likely from 3d and 4p orbital hybridization.

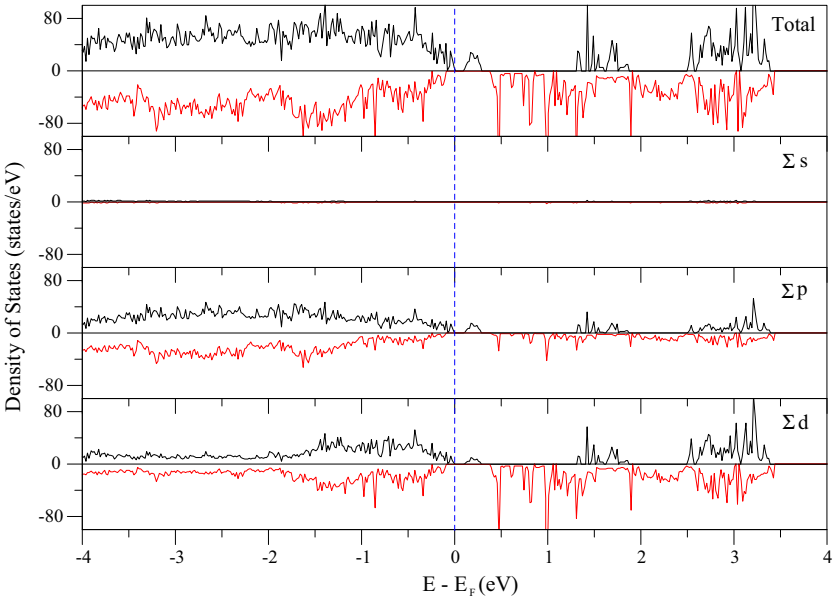

Fig. 5. Total DOS and PDOS in the sum of s, p, d orbitals of the CCO–Fe system.

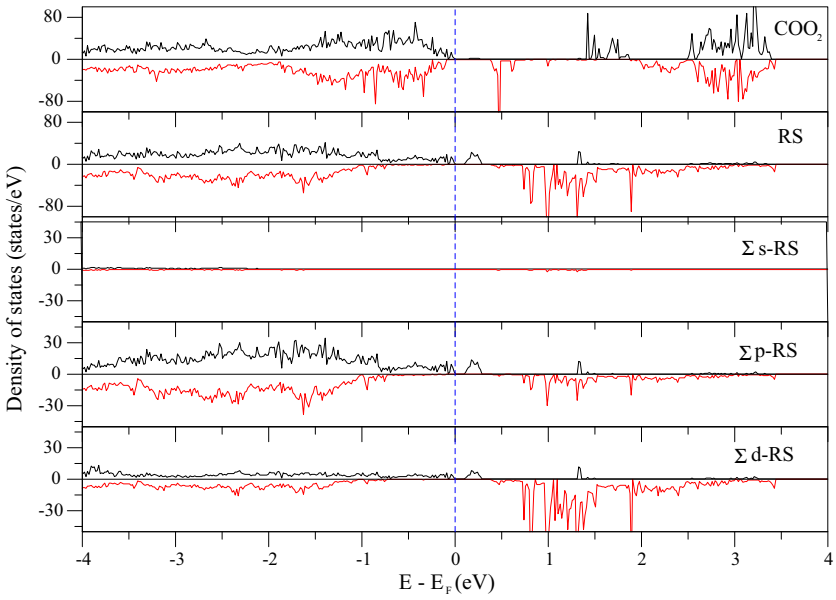

Fig. 6. PDOS of CCO–Fe in the RS and CoO_2 subsystem, and the sum of s, p, d, orbitals in the RS layer.

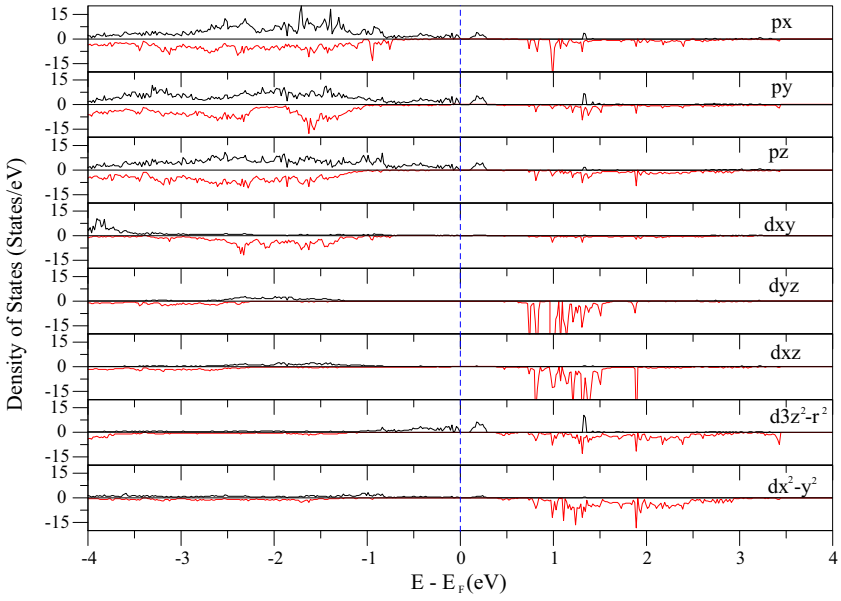

Fig. 7. PDOS projected into angular momentum resolved p and d orbitals in the RS layer of CCO–Fe.

A generally accepted picture of the electronic transport in the CCO system is that the conduction is limited in the CoO_2 layer and the RS layer acts as a charge reservoir providing carriers as needed [5,11,14]. Indeed, there is a direct observation of the charge transfer between the RS and CoO_2 layers [37]. This supports the idea that, for the p-type semiconducting CCO, holes are transferred from the RS layer to the CoO_2 layer and make contribution to electronic conduction. Our calculation has shown that the addition of Fe atoms generate an intermediate band with a small gap of only ~0.1 eV. This band would act as a hole source and enhance the hole concentration of the system, particularly at high temperature. The experimental results support this idea because the Hall measurement showed that the hole concentration increased for the Fe-doped CCO sample [20,23].

The angular momentum projections of the p and d orbitals in the RS layer of CCO–Fe are shown in Fig. 7. It can be clearly seen that the extra spin-up states in the conduction band is the combination of p and d orbitals. For the p orbital electrons, the states are equally divided among the projection in *x*, *y* and *z* direction whereas it is mainly due to $d_{3Z^2-r^2}$ for the d orbital electrons. On the other hand, the angular momentum projections of the d orbitals PDOS in the CoO_2 layer are shown in Fig. 8. When compared to the undoped CCO (Fig. 4), the main features are very similar except the shift of E_F to the higher level. This shift causes the Fermi level to be above the t_{2g} band in both spin channels and be right at the edge of the spin-up e_g band. For the undoped CCO, we have discussed earlier that the configuration of the d band in the CoO_2 sublattice is a result of the combination of Co^{3+} and Co^{4+}. The shift to the

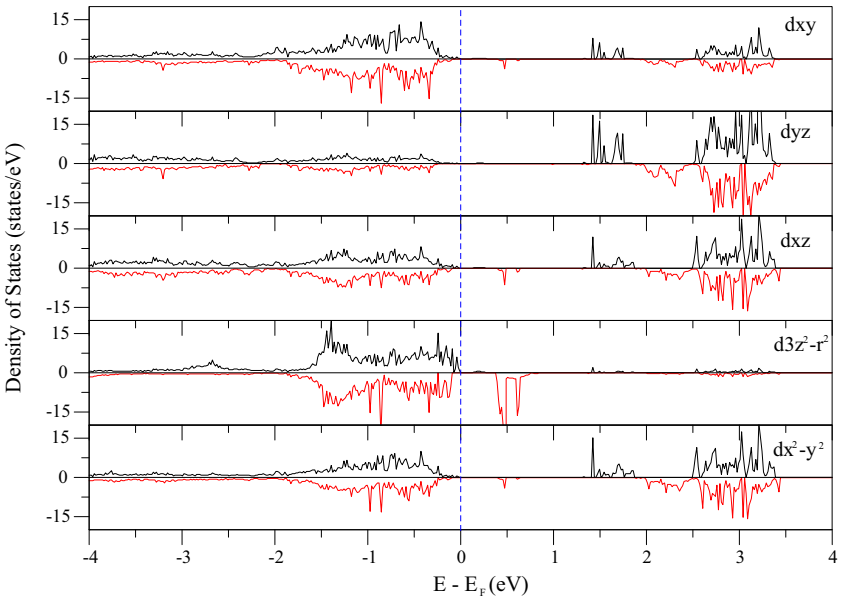

Fig. 8. PDOS projected into angular momentum resolved d orbitals in the CoO_2 layer of CCO–Fe.

higher level of E_F, particularly for the e_g band, would lead to the reduction of Co^{4+} ions. Theoretically, the thermopower of the CoO_2 compound family ($NaCo_2O_4$, $Ca_3Co_4O_9$, etc.) at the high-temperature limit has been estimated within the framework of the Heikes formula [17]:

$$S = -\frac{k_B}{e}\ln\left(\frac{g_3}{g_4}\frac{x}{1-x}\right) \quad (3)$$

where g_3, g_4 are the degeneracies of Co^{3+} and Co^{4+}, and x is the concentration of Co^{4+}. For the low-spin degeneracy of Co^{3+}, the thermopower is inversely proportional to the concentration of Co^{4+}. Our calculated results have shown that concentration of Co^{4+} is reduced up on doping Fe solute. This is, therefore, another implication for the increase of S in the Fe-doped sample. In fact, there have been a number of experimental works which explain the variation of S with doping in the CCO systems based on Eq. (3) [38–40].

The calculated magnetic moments of CCO–Fe are shown in Table 1. As explained in the experimental section, we test the effect of the initial magnetic moment of Fe. The result shows that for the 1.3 μ_B, the final magnetic moment are converged at the value of 2.89 μ_B in the RS layer, and −0.19 μ_B in the CoO_2 layer, and the magnetic moment of the Fe atom is converged at 3.25 μ_B. In the case of 4.0 μ_B initial moments, the final magnetic moments are very similar with the values in the RS and CoO_2 sublattices as 2.87 μ_B and −0.08 μ_B, respectively, and the final magnetic moment of the Fe atom is 3.44 μ_B. It can be seen that the results from both initial magnetic moments of Fe do not have much influence on the final state, i.e. both cases show very similar final value. This might be due to the low concentration of the Fe solute atom in the model (1 Fe atom in total 132 atoms). The total energy of the two systems having different initial magnetic moment of Fe is shown in Table 1. It can be seen that the total energy of the system with the intitial moment of 1.3 μ_B is lower than the other system by just 0.76 eV, indicating that the initial condition for the magnetic moment of Fe atom is not as important as in the case of the Co atoms. Anyhow, the DOS and PDOS shown in Figs. 2–4 are calculated from the energetically lower state, i.e. the 1.3 μ_B initial condition.

Fig. 9 shows the electron density map in the *ac* plane of the CCO–Fe. It can be clearly seen that the electron concentration is localized in each layer. There is a clear gap of the electron density between the RS and the CoO_2 layers. That means that even with Fe

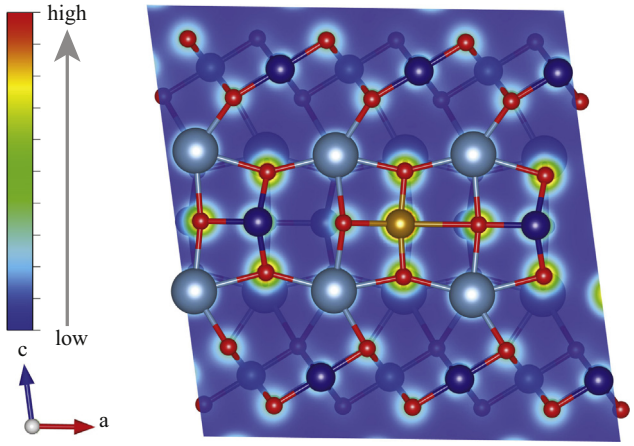

Fig. 9. Charge density in the *ac* plane of the CCO–Fe system.

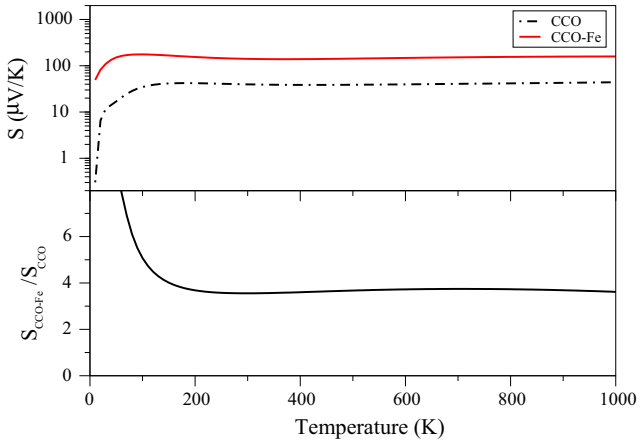

Fig. 10. Comparison of the calculated thermopower between the undoped and Fe-doped systems.

doping, the electronic transport is still confined to each sublattice. The CoO_2 layer is the conduction path for holes transport whereas the RS layer is the source for supplying holes.

To quantitatively compare the values of thermopower from the calculated electronic structure of the two systems, the Botztrap package based on semi-classical Boltzmann transport theory was employed and the result is shown in Fig. 10. It is clearly seen that the thermopower of the Fe-doped system is significantly higher than the undoped one. The bottom panel of Fig. 10 shows the ratio of S_{CCO-Fe}/S_{CCO} for which the value is nearly 4 times at temperature above 200 K. The increase of the Seebeck coefficient in the Fe-doped system from our calculation is supported by the experiments with comparable magnitude (of the order of 10^{-4} V/K) at the high temperature limit [22,23,27].

4. Conclusion

In this work, we have used the DFT + U calculation to determine the electronic structure of CCO and CCO–Fe. For the CCO case, the main contribution near E_F is from the p–d orbital of the CoO_2 layer. The Fermi level falls into the valley of the valence band. In the CoO_2 sublattice, Co^{3+} has a low spin state configuration whereas Co^{4+} shows a mixed spin state. Most of the main feature of the DOS is very similar to the previous report [16], except for the d-states projection. For the CCO–Fe case, the main differences from CCO are (1) the shift of E_F to the higher level, and (2) the additional states $\sim$0.1 eV above E_F in the RS sublattice. The former effect has an implication on the thermopower. When the E_F is right at the edge of the band where the slope is high, it enhances the thermopower. Furthermore, the projection of d orbital in the CoO_2 layer shows the reduction in Co^{4+} ions when the E_F is relatively higher. The reduction in Co^{4+}, according to the Heikes formula, would lead to the increase in S. The latter effect is interpreted as the intermediate state which acts as the hole source. The holes could be transferred from the RS layer and be electrically conductive in the CoO_2 layer. In conclusion, our theoretical work has shown an improvement in the thermoelectric properties for CCO–Fe which is reasonably agreed with the past experiments.

Acknowledgments

This work is supported by the Thailand Research Fund (TRF) under the Research Grant for New Scholar (TRG5780050), the TRF in cooperation with the Commission on Higher Education (MRG5680159), and the TRF under the TRF Senior Research Scholar (RTA5680008).

References

[1] T.M. Tritt, M.A. Subramanian, MRS Bull. 31 (2006) 188.
[2] I. Terasaki, Y. Sasago, K. Uchinokura, Phys. Rev. B 56 (1997) R12685.
[3] M. Shikano, R. Funahashi, Appl. Phys. Lett. 82 (2003) 1851.
[4] P. Limelette, V. Hardy, P. Auban-Senzier, D. Jerome, D. Flahaut, S. Hebert, R. Fresard, C. Simon, J. Noudem, A. Maignan, Phys. Rev. B 71 (2005) 233108.
[5] A.C. Masset, C. Michel, A. Maignan, M. Hervieu, O. Toulemonde, F. Studer, B. Raveau, Phys. Rev. B 62 (2000) 166.
[6] J. Sugiyama, C. Xia, T. Tani, Phys. Rev. B 67 (2003) 104410.
[7] H.W. Eng, P. Limelette, W. Prellier, C. Simon, R. Fresard, Phys. Rev. B 73 (2006).
[8] N. Prasoetsopha, S. Pinitsoontorn, P. Thongbai, T. Yamwong, Electron. Mater. Lett. 9 (2013) 347.
[9] S. Lambert, H. Leligny, D. Grebille, J. Solid State Chem. 160 (2001) 322.
[10] C.D. Ling, K. Aivazian, S. Schmid, P. Jensen, J. Solid State Chem. 180 (2007) 1446.
[11] Y. Miyazaki, M. Onoda, T. Oku, M. Kikuchi, Y. Ishii, Y. Ono, Y. Morii, T. Kajitani, J. Phys. Soc. Jpn. 71 (2002) 491.
[12] H. Muguerra, D. Grebille, F. Bouree, Acta Crystallogr. B 64 (2008) 144.
[13] G.D. Tang, H.H. Guo, T. Yang, D.W. Zhang, X.N. Xu, L.Y. Wang, Z.H. Wang, H.H. Wen, Z.D. Zhang, Y.W. Du, Appl. Phys. Lett. 98 (2011) 202109.
[14] T. Takeuchi, T. Kondo, T. Takami, H. Takahashi, H. Ikuta, U. Mizutani, K. Soda, R. Funahashi, M. Shikano, M. Mikami, S. Tsuda, T. Yokoya, S. Shin, T. Muro, Phys. Rev. B 69 (2004) 125410.
[15] R. Asahi, J. Sugiyama, T. Tani, Phys. Rev. B 66 (2002) 155103.
[16] A. Rebola, R. Klie, P. Zapol, S. Ogut, Phys. Rev. B 85 (2012) 155132.
[17] W. Koshibae, K. Tsutsui, S. Maekawa, Phys. Rev. B 62 (2000) 6869.
[18] S. Butt, Y.C. Liu, J.L. Lan, K. Shehzad, B. Zhan, Y. Lin, C.W. Nan, J. Alloys Compd. 558 (2014) 277.
[19] S. Pinitsoontorn, N. Lerssongkram, N. Keawprak, V. Amornkitbamrung, J. Mater. Sci. – Mater. Electron. 23 (2012) 1050.
[20] N. Prasoetsopha, S. Pinitsoontorn, A. Bootchanont, P. Kidkhunthod, P. Srepusharawoot, T. Kamwanna, V. Amornkitbamrung, K. Kurosaki, S. Yamanaka, J. Solid State Chem. 204 (2013) 257.
[21] N. Prasoetsopha, S. Pinitsoontorn, T. Kamwanna, V. Amornkitbamrung, K. Kurosaki, Y. Ohishi, H. Muta, S. Yamanaka, J. Alloys Compd. 588 (2014) 199.
[22] Y. Wang, Y. Sui, P. Ren, L. Wang, X.J. Wang, W.H. Su, H.J. Fan, Chem. Mater. 22 (2010) 1155.
[23] Y. Wang, Y. Sui, X. Wang, W. Sui, X. Liu, J. Appl. Phys. 107 (2010) 033708.
[24] Q. Yao, D.L. Wang, L.D. Chen, X. Shi, M. Zhou, J. Appl. Phys. 97 (2005) 103905.
[25] L.X. Xu, F. Li, Y. Wang, J. Alloys Compd. 501 (2010) 115.
[26] Y. Wang, Y. Sui, J. Cheng, X.J. Wang, J.P. Miao, Z.G. Liu, Z.N. Qian, W.H. Su, J. Alloys Compd. 448 (2008) 1.
[27] C.J. Liu, L.C. Huang, J.S. Wang, Appl. Phys. Lett. 89 (2006) 204102.
[28] G. Kresse, J. Furthmuller, Comput. Mater. Sci. 6 (1996) 15.
[29] D.M. Ceperley, B.J. Alder, Phys. Rev. Lett. 45 (1980) 566.
[30] S.L. Dudarev, G.A. Botton, S.Y. Savrasov, C.J. Humphreys, A.P. Sutton, Phys. Rev. B 57 (1998) 1505.
[31] P.E. Blochl, Phys. Rev. B 50 (1994) 17953.
[32] H.J. Monkhorst, J.D. Pack, Phys. Rev. B 13 (1976) 5188.
[33] S. Pinitsoontorn, N. Prasoetsopha, P. Srepusharawoot, A. Bootchanont, P. Kidkhunthod, T. Kamwanna, V. Amornkitbamrung, K. Kurosaki, S. Yamanaka, Phys. Status Solidi A 211 (2014) 1732.
[34] T. Wu, T.A. Tyson, J.M. Bai, K. Pandya, C. Jaye, D. Fischer, J. Mater. Chem. C 1 (2013) 4114.
[35] T. Mizokawa, L.H. Tjeng, H.J. Lin, C.T. Chen, R. Kitawaki, I. Terasaki, S. Lambert, C. Michel, Phys. Rev. B 71 (2005) 193107.
[36] Y. Wakisaka, S. Hirata, T. Mizokawa, Y. Suzuki, Y. Miyazaki, T. Kajitani, Phys. Rev. B 78 (2008) 235107.
[37] G. Yang, Q. Ramasse, R.F. Klie, Phys. Rev. B 78 (2008) 153109.
[38] N.V. Nong, C.J. Liu, M. Ohtaki, J. Alloys Compd. 509 (2011) 977.
[39] G.D. Tang, F. Xu, D.W. Zhang, Z.H. Wang, Ceram. Int. 39 (2013) 1341.
[40] F.P. Zhang, X. Zhang, Q.M. Lu, J.X. Zhang, Y.Q. Liu, G.Z. Zhang, Solid State Sci. 13 (2011) 1443.